NO adsorption/desorption pathways over Pd/SSZ-13 low temperature NO$_x$ adsorbers investigated by *operando* FT-IR spectroscopy and microreactor study

R. Matarrese [a], L. Castoldi [a], S. Morandi [b], P. Ticali [b], M.C. Valsania [b], L. Lietti [a],[*]

[a] *Laboratory of Catalysis and Catalytic Processes, Department of Energy, Politecnico di Milano, Milano 20156, Italy*
[b] *Department of Chemistry, NIS and INSTM Centers, Università di Torino, 10125 Torino, Italy*

A R T I C L E   I N F O

Keywords:
Pd-SSZ-13
Pd-promoted zeolites
Cold-start
Low-temperature NO$_x$ adsorbers
PNA

A B S T R A C T

In this study a Pd-doped SSZ-13 zeolite sample is synthesized, characterized and evaluated for potential use in the low-temperature NO$_x$ adsorption. TEM/HR-TEM and in-situ CO/NO adsorptions followed by FT-IR spectroscopy are used to gain information on the nature and accessibility of the Pd sites. It is found that over the calcined sample Pd is present as isolated Pd$^+$ and Pd^{2+} cations formed by ion exchange with the Brønsted acid sites of the zeolite, and as Pd$^+$ and Pd^{2+} species belonging to PdO$_x$ particles on the external surface of the zeolite. Isolated Pd^{2+} ions prevail on the calcined fresh sample. The NO$_x$ adsorption/desorption performances, investigated by microreactor studies and *operando* FT-IR under relevant operating conditions, indicate that significant amounts of NO are stored on the catalyst (i.e. ca. 80–95 μmol/g$_{cat}$ of NO$_x$ in the temperature range 50–150 °C) which suggests the participation in the NO$_x$ uptake of both isolated Pd^{n+} sites and PdO$_x$ particles. NO is adsorbed as nitrosyls (anhydrous and hydrated) over both Pd^{2+} and Pd$^+$; at low temperatures the formation of nitrates is also observed. The NO uptake as nitrosyls occurs with evolution of NO$_2$ according with a NO storage mechanism which implies (i) the initial adsorption of NO on Pd^{2+}, followed by (ii) the reduction of Pd^{2+} to Pd$^+$ by NO accompanied by NO$_2$ release and eventually (iii) the adsorption of NO on Pd$^+$. The suggested interconversion of Pd^{2+} into Pd$^+$ during NO adsorption is herein discussed based on FT-IR evidences. The stored NO$_x$ species are decomposed upon heating; nitrates are responsible for low temperature NO$_x$ desorption (below 200 °C), whereas nitrosyls show much higher stability and lead to a high temperature NO desorption (above 200 °C). The presence of NO$_2$ in the feed stream increases the NO$_x$ adsorption capacity and results in the formation of mainly surface/bulk nitrates and nitro-compounds at the expense of nitrosyls.

1. Introduction

NO$_x$ emissions from vehicle exhausts are reduced using three-way catalysts (TWC) and selective catalytic reduction (SCR) / lean NO$_x$ trap (LNT) catalysts for stoichiometric gasoline and lean-burn diesel engines, respectively. However, the mitigation of NO$_x$ emission for the current NO$_x$ control technologies, particularly for lean-burn engines, is challenging at cold start, i.e. when the catalytic converter temperature is below 200 °C [1–4]. This has forced the tightening of environmental regulations to the cold start period both in terms of pollutant limits and testing procedures for certification and compliance [5].

One of the most promising approach to address cold-start NO$_x$ emission is to employ passive NO$_x$ adsorbers (PNA), also referred as low-temperature NO$_x$ adsorbers (LTNA), which are designed to adsorb NO$_x$ upstream of the main catalytic converter (e.g. SCR, LNT) during the cold-start period, and to thermally release the stored NO$_x$ at higher temperatures, when the downstream catalytic converters become active [6–10]. Among the various investigated catalyst formulations, Pd containing zeolites emerged as most promising thanks to their higher trapping efficiency, storage capacity and superior sulphur resistance if compared to ceria/alumina-based systems. In particular, small-pore Pd-CHA(SSZ-13) has attracted increasing attention because of proper NO$_x$ storage capacity, NO$_x$ desorption temperature and hydrothermal stability [11–15], although the use of other zeolite frameworks (e.g. ferrierite) has been suggested [16,17].

Despite Pd-supported zeolites have been widely investigated, the

reaction pathways operating during NO_x adsorption and particularly the nature of the NO_x adsorption active sites are still under debate. Zheng et al. [18] investigated the structure and the adsorption behavior of several Pd-zeolites (i.e. Beta, ZSM-5, and SSZ-13) and reported the existence of a variety of Pd NO-adsorption sites, ranging from isolated Pd cations into the zeolite framework to PdO_x clusters on the external zeolite surface. This was also supported by other literature reports [10, 19–21], although isolated Pd cations emerged as the most efficient NO storage sites [11,18,19,22–24]. With the aid of FT-IR spectroscopy, and supported by DFT calculations, Szanyi and co-workers [12,22] indicated the role of both Pd^{2+} and Pd^+ ionic sites as storage centres leading to the formation of Pd^{2+} and Pd^+ nitrosyl complexes upon NO adsorption. They also showed that the NO adsorption involves not only simple chemical adsorption but also redox reaction pathways via the reduction of Pd^{2+} in the form of $[Pd(OH)]^+$ to Pd^+ sites, but also of PdO_2 to PdO clusters, by NO forming NO_2 [18]. The reduction of Pd cations (i.e. Pd^{2+} and PdO_2) by NO serving as reductant was also supported by Harold and co-workers [25–27] and recently by Kim et al. [28]. According to a combined experimental and modeling study, Pd^{2+} and Pd^+ sites were indicated to be both involved in the adsorption of NO, although Pd^+ sites have been indicated as the primary NO storage site. In fact, based on NO adsorption and TPD experiments under different operating conditions, Tronconi et al. [29] were able to demonstrate that the NO storage is favored under reducing conditions (e.g. in the presence of CO), and that the stability of adsorbed NO is decreased under oxidizing conditions. The role of Pd^+ species in the formation of strongly adsorbed NO species was also supported by Kaushik et al. [30] by means of DFT simulations. At variance, some IR studies indicated Pd^{2+} sites as active NO storage sites, even in the presence of CO, i.e. a strong reducing agent [12, 31–33]. In particular, Song et al. [32] suggested Pd^{2+} ions as the primary NO adsorption sites even with gases containing CO and water, where Pd can be easily reduced; Mandal et al. [33], based on DFT and spectroscopic results, indicated that Pd complexes are primarily manifested as mobile and H_2O-solvated Pd^{2+} species under conditions of practical relevance.

With specific regards to Pd^+ species, their existence in the as-prepared and pretreated Pd/zeolites remains debated. According to XPS and EXAFS analyses, several reports showed Pd^{2+} as the dominant oxidation state of palladium after calcination in oxygen of as-prepared catalysts [19,22,23,25,27,34]. Besides, according to FT-IR/DRIFTS results with CO as probe molecule at low temperature the existence of also Pd^+ ions has been reported [11,18,35,36]. DFT calculations by Mandal et al. [33] indicated Pd^{2+} cations at Al pair sites in the 6-membered ring of CHA as the most thermodynamically stable Pd species. Conversely, DFT studies reported by Bell and co-workers [37] showed that the speciation of Pd (i.e. the presence of both Pd^{2+} and Pd^+ cations) strongly depends on the different Al arrangement within the zeolite framework (i.e. in both the 6- and 8-membered ring of the CHA) and on the operating conditions as well (i.e. temperature and exposure to water).

Based on these premises, the present study was undertaken to provide further piece of evidence on the chemistry involved in the NO_x adsorption phenomena on Pd/SSZ-13, particularly focusing on the nature, stability and reactivity of the adsorbed NO_x species. For this purpose, TEM characterization and in-situ CO/NO adsorptions followed by FT-IR spectroscopy were used to gain information on the nature and accessibility of the Pd sites under controlled conditions. Then, *operando* FT-IR spectroscopy and micro-reactor reactivity studies were carried out trying to spread light on the nature/stability of the adsorbed NO_x species and on the mechanisms of both the NO_x adsorption and desorption. To this end, the NO_x trapping and release characteristics were evaluated under simulated exhaust conditions, i.e. in the presence of both H_2O and CO_2, at different adsorption temperature and also in the presence of NO_2, i.e. another realistic component in the engine exhausts.

2. Experimental

2.1. Catalyst preparation

The Pd-doped chabazite used in this study (Pd_1/SSZ-13, nominal Pd loading 1% w/w) was prepared starting from a commercial zeolite (ACS Chemical, Si/Al = 10–15), available in its H-form. The catalyst sample was prepared by impregnation of the zeolite support using an aqueous $Pd(NO_3)_2$ solution prepared starting from a commercial 4.5% Pd solution (Sigma-Aldrich). The impregnation was carried out by using an impregnating volume 50% in excess with respect to the zeolite pore volume. The resulting slurry was stirred at r.t. overnight and eventually dried under vacuum at 80 °C [38]. The dried precursor was calcined at 750 °C for 2 h with a two-ramp heating program, from room temperature up to 500 °C (rate: 1 °C/min, hold at 500 °C 3 h) and then from 500 °C up to 750 °C (rate 5 °C/min, hold at 750 °C 2 h) to obtain the fresh calcined sample.

2.2. Catalyst characterization

The Pd loading was analyzed by SEM-EDX; an actual content of 1.14% w/w has been estimated.

BET analysis were performed by adsorption-desorption of nitrogen at − 196 °C using a Micrometrics Tristar 300 instrument. Prior to the measurement all samples were outgassed under vacuum at 350 °C for 1 h. The specific surface area of the bare SSZ-13 is 460 m^2/g_{cat}; the addition of Pd does not significantly modify this value.

Information about the crystalline structure of the bare and Pd-doped zeolite was obtained from powder X-ray diffraction (XRD) using a Bruker D8 diffractometer with Cu Kα radiation. The XRD patterns were taken in the range of 10–50° (2 θ) with a step size of 0.05° at a speed of 12.5°/min. XRD patterns obtained on the parent SSZ-13 is in agreement with the diffraction patterns for CHA zeolite framework [39]. The addition of Pd neither modifies the zeolite structure, nor leads to the appearance of new peaks in the spectra.

Transmission Electron Microscopy (TEM) and High Resolution (HR)-TEM analyses were performed by using a side entry Jeol JEM 3010 (300 kV) microscope equipped with a LaB$_6$ filament. The samples were deposited on a copper grid, coated with a porous carbon film; the digital micrographs were acquired by an Ultrascan 1000 camera and the images were processed by Gatan digital micrograph. The characterization was performed on the calcined Pd_1/SSZ-13 oxidized at 500 °C with 40 mbar of O_2, reduced at 500 °C with 40 mbar of H_2 and eventually re-oxidized at 500 °C with 40 mbar of O_2.

The metal phase properties and the acidic character of the sample after different treatments were determined by FT-IR spectroscopy upon adsorption of probe molecules (CO, NH_3, NO) in static conditions at room temperature (r.t.) and also at liquid nitrogen temperature (T_{N2}) in the case of CO. Absorption/transmission IR spectra were run on a Perkin-Elmer FT-IR 2000 spectrophotometer equipped with a Hg-Cd-Te cryodetector, working in the range of wavenumbers 7200–1000 cm^{-1} at a resolution of 2 cm^{-1} (number of scans, ~60). For IR analysis, calcined powder sample was pelletized in self-supporting disk (10–15 mg cm^{-2}) and placed in a quartz IR cell allowing thermal treatments in vacuo or under controlled atmosphere. Pellet was activated at 500 °C by oxidizing or reducing treatment in O_2 (40 mbar) or H_2 (40 mbar), respectively. After the oxidizing treatment the sample was cooled down to r.t. in oxygen, conversely, after the reducing treatment, H_2 was outgassed at 500 °C and then the sample was cooled down to r.t. IR spectra were recorded at r.t. before and after interaction with CO, NH_3, NO and after subsequent evacuation at r.t. In the figures, spectra are reported as difference spectra, where the reference spectrum is that of the sample after the activation, before the gas admission.

2.3. Reactivity studies

NO$_x$ adsorption experiments were conducted both in a microreactor apparatus and in an *operando* FT-IR cell (#CSX, AABSPEC). In the first case, 100 mg of the calcined powdered catalyst, sieved at 70–100 μm, were loaded in a quartz microreactor with an internal diameter of 8 mm.

The outlet of the reactor was directly connected to a mass spectrometer (ThermoStar 200, Pfeiffer Vacuum) and a UV-analyzer specific for NO, NO$_2$, NH$_3$ (Limas 11HW, ABB) for continuous on-line analysis, and to a micro gas-chromatograph (3000 A, Agilent) for periodic analysis. In a typical experiment, the sample was pre-treated in the microreactor under a flow (100 Ncm^3/min) of O$_2$ (3% v/v), CO$_2$ (2% v/v), H$_2$O (2.5%
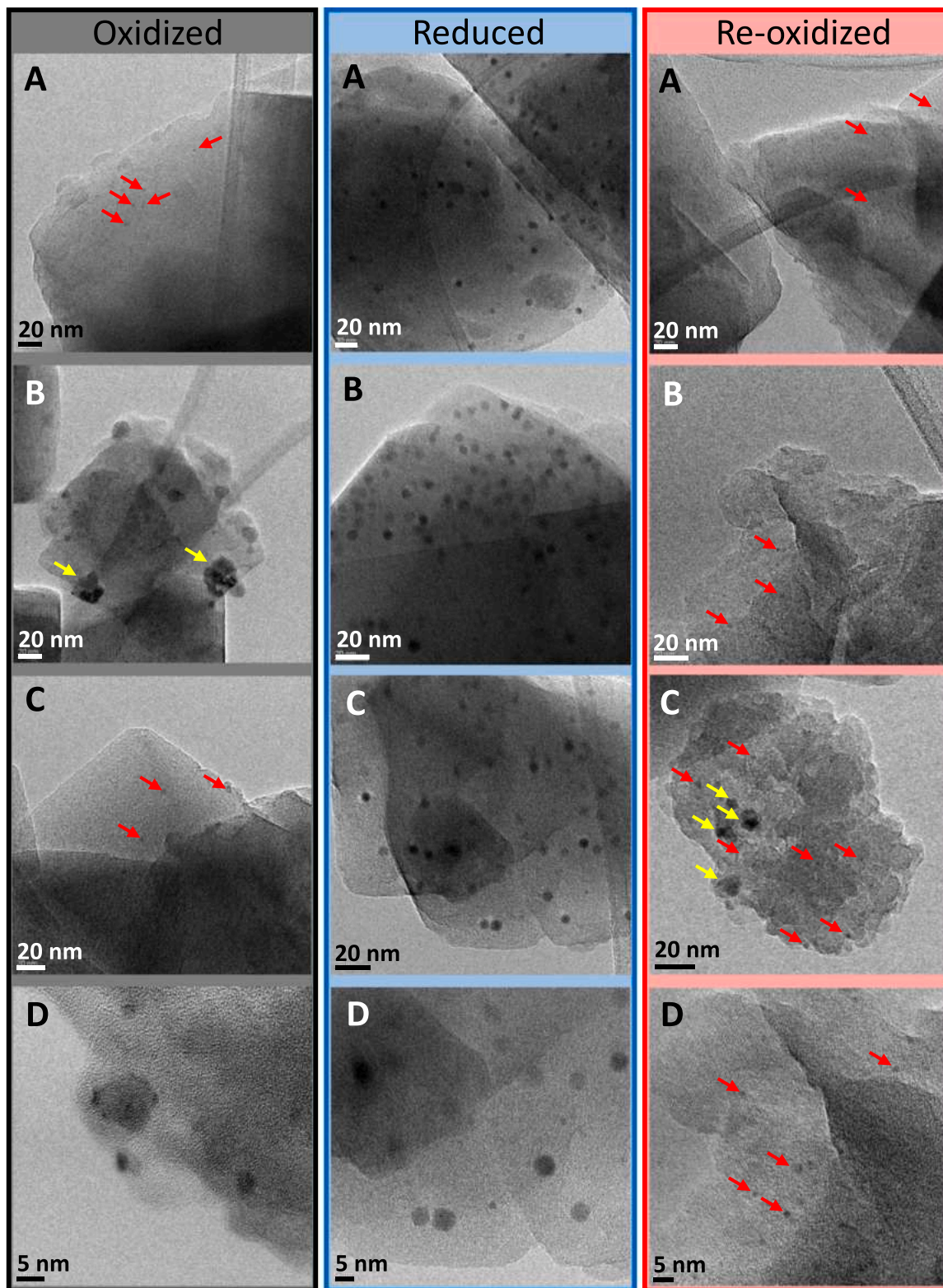

Fig. 1. - TEM and HR-TEM images of Pd$_1$/SSZ-13 oxidized in O$_2$ (40 mbar) at 500 °C, reduced in H$_2$ (40 mbar) at 500 °C and re-oxidized in O$_2$ (40 mbar) at 500 °C. Red arrows: some less recognizable Pd particles; yellow arrows: Pd particle aggregates.

v/v) (balance He) at 500 °C for 30 min. Then the catalyst was cooled down to the selected adsorption temperature and 300 ppm of NO were step-wise added to the gas mixture for 75 min (adsorption phase). Then, the NO supply was stopped and the catalyst was heated under temperature programming (TPD) up to 500 °C (heating rate 10 °C/min). The experiments were carried out by varying the adsorption temperature in the range 50–150 °C.

The amounts of NO_x stored on the catalyst surface upon NO admission have been evaluated both from the difference between the reactor outlet and inlet NO_x concentration traces (this latter obtained from an inert tracer) during the adsorption phase, and from the amount of NO_x desorbed during the subsequent TPD experiment. In both cases very similar quantities were obtained, as expected, with N-balance always closing within ± 5%. Accordingly, in the following the amounts of NO_x stored will be estimated from the NO_x desorption trace.

The effect of the NO_2 presence during the NO_x adsorption was also investigated. In this case the NO_x adsorption experiments were performed by adding NO_2 (50 ppm or 100 ppm) to the NO/O_2 mixture while keeping constant at 300 ppm the total NO_x concentration.

In the case of the *operando* FT-IR cell, the catalyst was formed in self-supported wafers (ca 0.10 mg cm^{-2}) and loaded in the FT-IR cell reactor. The IR spectra (reported as difference spectra, using as reference the spectrum obtained after the pre-treatment) were collected with a FT-IR Vertex 70 (Bruker, Billerica, MA, USA) equipped with a MCT cryodetector spectrometer with 4 cm^{-1} spectral resolution. The outlet of the FT-IR cell was connected to a to a mass spectrometer (ThermoStar 200, Pfeiffer Vacuum) for gas analysis. The experimental procedure and parameters adopted in the *operando* FT-IR cell were kept as much as possible identical to that used for the microreactor rig. However, the space velocity was higher (almost twice) in the *operando* cell due to technical limitations in the minimum flow rate (25 Ncm^3/min). Also, the water content was slightly lower (~ 1.5% vs. 2.5% v/v).

3. Results and discussion

3.1. Catalyst characterization

3.1.1. TEM and HR-TEM analysis

Fig. 1 displays TEM (panels A, B and C) and HR-TEM images (panels D) of the calcined Pd$_1$/SSZ-13 after the first oxidation, reduction and re-oxidation treatments at 500 °C. On the freshly oxidized sample PdO$_x$ particles are observable, indicating that not all the Pd deposited upon the catalyst preparation is well dispersed. It is important to underline that the zeolite porosity is too small to host particles detectable by TEM and HR-TEM; as a consequence, PdO$_x$ particles visible in the images are on the external surface of the zeolite. Red arrows enlighten some of the smallest and less recognizable particles, taken as example. The freshly oxidized sample shows regions with homogeneously distributed small PdO$_x$ particles (panels A and C) and other regions with bigger particles (panel B): the particle size distribution is very broad, being from about 1 nm to about 30 nm. However, particles with dimensions of about 30 nm (enlightened by yellow arrows in panel B) appears to be aggregates of smaller particles for the following reasons: (i) they show irregular shapes; (ii) they display regions with different contrast that enlightens different thicknesses. The major part of the particles with regular shape and homogeneous contrast is in the range 1–20 nm.

For the reduced sample, the contrast difference between Pd particles and the zeolitic support is more marked than that observed after oxidation, confirming the PdO$_x$ and Pd^0 nature for the particles observed on the oxidized and reduced sample, respectively. Reduced sample shows narrower Pd particle size distribution, being the dimensions in the range 1–7 nm. It is worth of note that the reducing treatment, on one hand, disrupts the aggregates enlighten by yellow arrows in the images of the freshly oxidized sample, on the other hand, causes the aggregation of the smallest particles enlighten by red arrows in the images of the freshly oxidized sample.

After re-oxidation, particle dimensions are in the range 1–15 nm and some particle aggregates with dimensions bigger than 15–20 nm appear as in the case of the freshly oxidized sample (yellow arrows in panel C). However, differently from the freshly oxidized sample, the re-oxidized one shows less regions with particles bigger than 10 nm and with particle aggregates. Indeed, for the re-oxidized sample images in panels A, B and D are statistically more frequent than image in panel C. Accordingly TEM and HR-TEM images show that: (i) not all Pd is well dispersed on the surface; (ii) reduction treatment leads to Pd^0 particles with a different size distribution than that observed for PdO$_x$ particles after oxidation; (iii) the re-oxidation performed after the reduction treatment leads to a PdO$_x$ phase more spread than that observed for the freshly oxidized sample. These results point out the high surface mobility of Pd during thermal treatments, as also confirmed by FTIR results discussed below.

3.1.2. FT-IR characterization

3.1.2.1. CO adsorption.
The nature and accessibility of the Pd sites have been characterized by CO adsorption at r.t. followed by FT-IR spectroscopy. This technique provides complementary information on the nature of Pd sites with respect to TEM and HR-TEM measurements in that finely dispersed PdO$_x$ and Pd^0 phases, and isolated species as well, are obviously not detectable by electron microscopy.

In Fig. 2 FT-IR spectra obtained upon CO adsorption up to 20 mbar at r.t. on the calcined Pd$_1$/SSZ-13 catalyst pre-treated at 500 °C in O$_2$ (40 mbar) are displayed. The spectra are characterized by complex envelopes of bands that increase in number and intensity upon increasing CO pressure. The bands are related to many Pd carbonyl species; the number of different absorptions reflects the presence of Pd species in different oxidation (Pd^{2+} and Pd$^+$) and coordination (isolated ions and particles) states. On the basis of literature data [40,41], it is possible to distinguish two groups of bands: one in the spectral region 2220–2170 cm^{-1}, related to linear carbonyls of Pd^{2+}, and the other one in the spectral region 2170–2110 cm^{-1} that we relate to linear carbonyls of Pd$^+$; in both cases the bands are associated to isolated ions and particles. However, we noted that recently some authors assigned bands in the region 2170–2110 cm^{-1} to carbonyls of Pd^{2+} ions [22,34,36]. This was based on EXAFS analyses apparently showing that only Pd^{2+} ions exist after oxidation treatment and that CO can hardly reduce Pd^{2+} to Pd$^+$. At variance, as will be discussed in the following, taking into account the nature of Pd-CO bond, i.e. σ-donation and π-backdonation contributions, and the CO coverage effect on some bands that demonstrates the formation of di-carbonyls, the presence of both Pd^{2+} and Pd$^+$ species can be suggested.
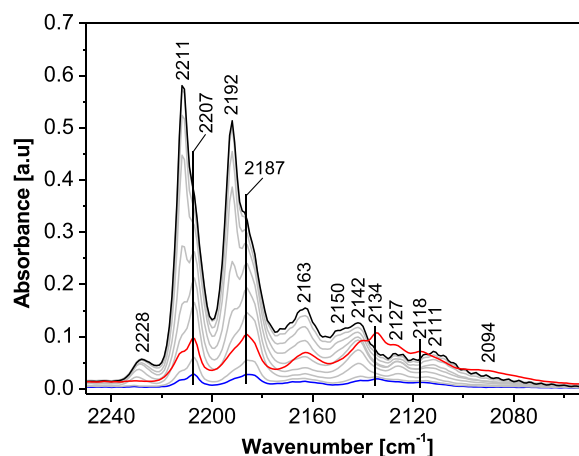

Fig. 2. - FT-IR spectra of CO adsorbed at r.t. at increasing pressure up to 20 mbar (from blue to black trace) on Pd$_1$/SSZ-13 catalyst pre-oxidized in O$_2$ (40 mbar) at 500 °C. Red trace: spectrum run after CO outgassing at r.t.

Moreover, some authors assigned bands at frequency higher than 2190 cm^{-1} to carbonyls of Pd^{3+}/Pd^{4+} [18,31,40], but, recently, some of them revised this assignment: by combining experimental and density functional theory studies, super electrophilic Pd^{2+} species, i.e. ion pairs with the negatively charged framework oxygen ions, was identified [34].

With regard to the spectral region 2220–2170 cm^{-1} associated to linear carbonyls of Pd^{2+}, it can be considered that, due to the σ-donation character of the Pd^{2+}-CO bond, the higher the band frequency, the more coordinatively unsaturated the site. In Fig. 2, at low pressure (blue trace) and after CO outgassing (red trace) the main bands are at 2207 and 2187 cm^{-1}. The band at 2187 cm^{-1} is assigned to CO adsorbed on Pd^{2+} sites belonging to PdO$_x$ particles, whose presence is enlightened by TEM and HR-TEM images (see Fig. 1). The band at 2207 cm^{-1} appears at low CO pressure, then almost disappears on increasing CO coverage and eventually appears again after outgassing (Fig. 2, red trace). At the same time bands at 2211 and 2192 cm^{-1} increase upon increasing CO pressure and eventually disappear after outgassing. This behavior allows to recognize the presence of mono-carbonyls (band at 2207 cm^{-1}) that become di-carbonyls upon increasing CO pressure (bands at 2211 and 2192 cm^{-1}, ν_{asym}(CO) and ν_{sym}(CO) modes, respectively) and come back to mono-carbonyl species upon outgassing. Di-carbonyls are usually formed on sites characterized by low coordination number. Thus, these bands are likely related to mono- and di-carbonyls of isolated Pd^{2+} ions formed by ion exchange with the Brønsted acid sites and stabilized by the zeolite framework [22,34].

Concerning the spectral region 2170–2110 cm^{-1}, that we relate to linear carbonyls of Pd$^+$, it can be considered that, due to the π-back-donation contribution to the Pd$^+$-CO bond, the lower the band frequency, the more coordinatively unsaturated the site. For this reason, the band at 2163 cm^{-1} is assigned to CO adsorbed on Pd$^+$ sites belonging to PdO$_x$ particles, whose presence is enlightened by TEM and HR-TEM images (see Fig. 1). Also in this region, the behavior of some bands upon changing the CO coverage allows to recognize the presence of mono-carbonyls that become di-carbonyls upon increasing CO pressure and come back to mono-carbonyl species after outgassing. Indeed, bands at 2134 and 2118 cm^{-1} appears at very low pressure (Fig. 2, blue trace), disappears on increasing pressure and then appears again after outgassing (Fig. 2, red trace). At the same time, upon increasing CO pressure, bands at 2150, 2142, 2127 and 2111 cm^{-1} increase and are eroded during the outgassing. Therefore, it is possible to recognize the presence of two mono-carbonyl species (bands at 2134 and 2118 cm^{-1}) that evolve in four bands related to di-carbonyls (bands at 2150, 2142, 2127 and 2111 cm^{-1}). This implies the presence of two different isolated Pd$^+$ sites formed by ion exchange with the Brønsted acid sites of the zeolite: indeed, Pd$^+$ can be located into 8 member-rings and 6-member rings of the zeolite framework [33,36,41].

The presence of carbonyl species that evolve in di-carbonyls upon increasing the CO pressure and come back to mono-carbonyl species after outgassing allows us to unambiguously identify the nature of the Pd species. In fact, although it has been suggested that all the bands in the spectral region 2170–2110 cm^{-1} are related to Pd^{2+} species [22,34], the region at lower frequency should be typical of PdO particles and not of Pd^{2+} isolated ions. However, this is in contrast with the observed presence of di-carbonyls (bands at 2150, 2142, 2127 and 2111 cm^{-1}) that are characteristic of isolated ions, which accordingly are Pd$^+$. This is further demonstrated by FT-IR measurements in the presence/absence of water that will be reported in a forthcoming paper (manuscript in preparation).

Outside the spectral regions of Pd$^{2+/+}$ carbonyls, the weak band at 2228 cm^{-1} can be assigned to carbonyls of extra-framework Al^{3+} [42]. Moreover, a broad absorption at 2094 cm^{-1} appears after CO outgassing (Fig. 2, red trace) and, referencing to literature data, it is a typical position of Pd^0 carbonyls [41,43]. The band at 2094 cm^{-1} becomes evident after outgassing: it is reasonable that some oxygen species on Pd particles are removed along with CO, which becomes CO$_2$, changing oxidized

Pd^{n+} sites into Pd^0 sites.

To investigate any reducing effect of CO at r.t., CO adsorption at liquid nitrogen temperature (T$_{N2}$) was performed on oxidized Pd$_1$/SSZ-13 and compared with the adsorption at r.t. (Fig. 3). At T$_{N2}$ CO is adsorbed not only on Pd sites, but also on the zeolite Brønsted acid sites and, moreover, it gives rise to a liquid-like phase inside the pores. These two phenomena are evidenced by the increase, at pressure higher than 0.1 mbar (spectra not reported), of two intense bands at about 2170 and 2140 cm^{-1}, which mask the bands related to Pd. For this reason, in Fig. 3 spectra recorded at 0.1 mbar of CO at r.t. (magenta trace) and T$_{N2}$ (green trace) were compared. The comparison well puts in evidence that bands in the 2170–2110 cm^{-1} range, related to Pd$^+$ sites, are present also at T$_{N2}$ with relative intensities similar to that observed at r.t. This means that, in the conditions here used, it is possible to exclude any reducing effect of CO at r.t, except for that observed during the outgassing. Therefore, it is possible to conclude that Pd$^+$ ions also exist, along with Pd^{2+} ions, even after oxidation at 500 °C.

Fig. 4 shows a comparison between the spectra obtained at the maximum CO pressure for the Pd$_1$/SSZ-13 sample oxidized and reduced at 500 °C. For the reduced sample (orange trace) the almost total absence of bands related to Pd carbonyls is evident: only very weak bands of un-reduced isolated Pd^{2+} ions stabilized by the zeolite framework are observed at 2211 and 2192 cm^{-1} (see inset in Fig. 4) [22,34]. A very weak band at 2228 cm^{-1} related to carbonyls of extra-framework Al^{3+} is also present [42]. The absence of bands related to Pd^0 carbonyls for the reduced catalyst would suggest a marked coalescence of Pd during the reduction pre-treatment, forming big reduced particles with very low amount of exposed surface sites; however, TEM images show Pd particles with size of about 1–7 nm that cannot justify the lack of detection of CO adsorption by IR. Indeed, Pd particle sizes exclude detection limit problems. It is not clear the reason for the complete inaccessibility of the surface sites on reduced Pd and the search for an explanation is not straightforward. Due to the reduction in hydrogen, the sites could be occupied by hydride species, even if the sample was outgassed at 500 °C and the Pd hydrides are not so stable. This point is still unclear and deserves further investigation.

The subsequent re-oxidation treatment leads again to the appearance of the Pd^{n+} carbonyl bands: the spectra obtained for CO adsorption are the same shown in Fig. 2.

The results discussed above call for a great stability of oxidized Pd^{n+} sites in the zeolite matrix in the presence of CO under dry conditions. At variance, it is documented in literature that oxidized Pd on basic supports is readily reduced to Pd^0 during contact with CO even at r.t., as reported by Bensalem et al. for Pd on ceria [44] and very recently by Ruzzi et al. for Pd supported along with Zn on a CeZrO$_x$ mixed oxide
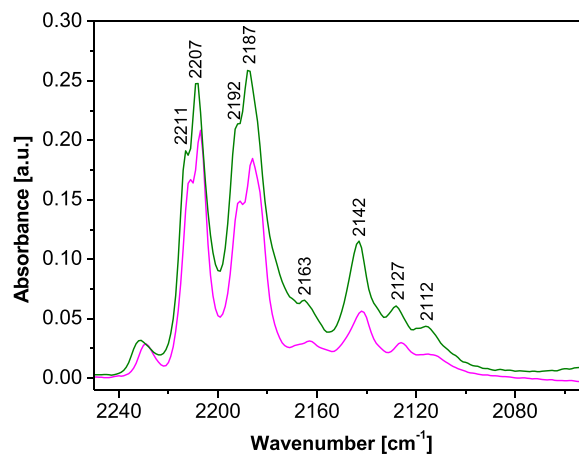

Fig. 3. - FT-IR spectra of CO (0.1 mbar) adsorbed at r.t. (magenta trace) and at T$_{N2}$ (green trace) on Pd$_1$/SSZ-13 catalyst pre-oxidized in O$_2$ (40 mbar) at 500 °C.
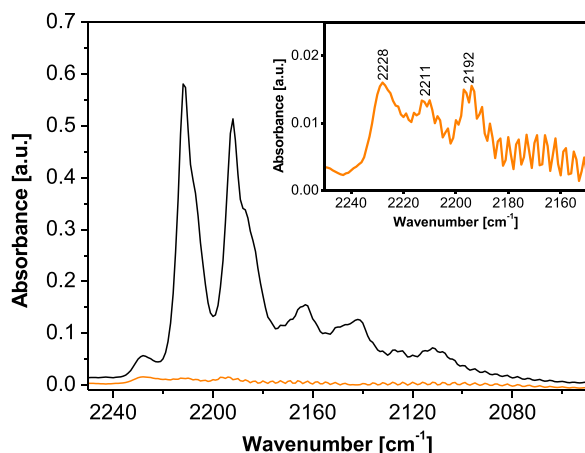
Fig. 4. - FT-IR spectra of CO (20 mbar) adsorbed at r.t. on Pd$_1$/SSZ-13 after different pretreatment: oxidation at 500 °C in 40 mbar of O$_2$ (black trace); reduction at 500 °C in 40 mbar of H$_2$ (orange trace). Inset: zoom of the orange trace (reduced sample).

Fig. 5. – FT-IR spectra after NH$_3$ (2 mbar) adsorption and subsequent evacuation at r.t. on Pd$_1$/SSZ-13 after different pretreatment: oxidation at 500 °C in 40 mbar of O$_2$ (black trace); reduction at 500 °C in 40 mbar of H$_2$ (orange trace).

[45]. In both cases the authors reported that only Pd^0 carbonyls are detected on the pre-oxidized samples and carbonate formation confirms the hypothesis of the PdO$_x$ reduction by CO followed by CO$_2$ formation. In our case, the zeolitic support strongly stabilizes not only ion-exchanged Pd^{n+}, but also PdO$_x$ particles on the external surface of the zeolite. These results are in agreement with those obtained very recently by Song et al. [32] that show how the reduction by CO of Pd ions exchanged in a SSZ-13 zeolite is limited under dry conditions even at temperature as high as 500 °C.

In conclusion, the results obtained by CO adsorption followed by FT-IR spectroscopy show that on the oxidized catalyst Pd is present as isolated Pd$^+$ and Pd^{2+} cations formed by ion exchange with the Brønsted acid sites of the zeolite, and as Pd$^+$ and Pd^{2+} species belonging to PdO$_x$ particles on the external surface of the zeolite, observed by TEM/HRTEM measurements. These oxidized species are stable under mild reducing conditions.

The quantification of the relative amounts of Pd$^+$ and Pd^{2+} species is not straightforward, but a rough estimation of their relative abundance can be attempted from the integrated intensities of the carbonyl peaks in the regions 2170–2100 (Pd$^+$) and 2220–2170 cm^{-1} (Pd^{2+}) (Fig. 2). By assuming the same absorption coefficient for Pd$^+$ and Pd^{2+} carbonyls, the Pd^{2+} / Pd$^+$ ratio is estimated to be near 1.3 at low CO coverage and 2.1 at high CO coverage. This indicates that Pd^{2+} is by far the most abundant Pd species over the oxidized sample.

At variance, the relative distribution of Pd ions into sites on the surface of particles and into isolated sites is not trivial due to a strong overlapping of the bands of these species, especially in the Pd^{2+} region (bands at 2187 and 2192 cm^{-1} for particles and isolated ions, respectively). However, it is well evident that both for Pd^{2+} and Pd$^+$ the bands related to carbonyls on particle sites (at 2187 and 2163 cm^{-1}, respectively) are markedly less intense than those associated to isolated ions, indicating the predominance of isolated ions. The prevalence of isolated (i.e. well dispersed) Pd species is also in line with the results of NO$_x$ adsorption experiments reported in the following, showing that about 85% of Pd is accessible for NO$_x$ uptake. Accordingly, it is concluded that the dominant Pd species on the investigated sample after oxidation at 500 °C are isolated Pd^{2+} ions.

3.1.2.2. NH$_3$ adsorption on Pd$_1$/SSZ-13. To further prove the ion exchange for the oxidized sample, the Brønsted/Lewis acidity was investigated using NH$_3$ as probe molecule. The ammonia adsorption at r.t. on Brønsted and Lewis acid sites gives ammonium ions and ammonia adducts, respectively, whose IR spectroscopic features are well discernable. Fig. 5 shows the spectra obtained after NH$_3$ interaction with
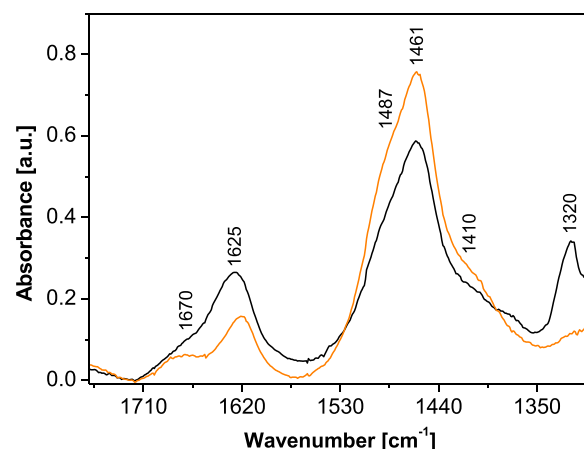
oxidized (black trace) and reduced (orange trace) Pd$_1$/SSZ-13. In order to remove weakly bonded NH$_3$, the spectra were recorded after interaction with ammonia (2 mbar) and subsequent outgassing at r.t.. The band at 1461 cm^{-1} and the shoulders at 1487 and 1410 cm^{-1} are assigned to the asymmetric bending of NH$_4^+$ ions formed by the interaction of ammonia with the Brønsted acid sites of the zeolite [46]. The presence of three components is related to the triple degeneracy of the asymmetric bending mode of free NH$_4^+$ ion: when the ion is adsorbed, the symmetry is lowered and the degeneration is lost [46]. The spectrum obtained over the reduced sample (orange trace) shows higher intensity of these bands with respect to the oxidized one (black trace). This means that for the reduced sample the amount of Brønsted acid sites is higher than that of the oxidized one. This is in agreement with the results obtained upon CO adsorption, which shows the almost complete removal of isolated Pd^{n+} ions, accounting for the increase of the Brønsted acid sites during treatment in hydrogen at 500 °C.

The band at 1320 cm^{-1} is present only for the oxidized sample and is assigned to δ_{sym}(N-H) mode of NH$_3$ bonded to Pd^{n+} ions [47]. The absence of this band for the reduced sample confirms the reduction of Pd^{n+} to Pd^0. The corresponding δ_{asym}(N-H) mode is at about 1670–1625 cm^{-1}, along with the δ_{sym}(N-H) mode of NH$_4^+$ formed on the Brønsted acid sites and the δ_{asym}(N-H) mode of ammonia bonded to extra-framework Al^{3+}.

3.1.2.3. NO interaction. Fig. 6 A shows the FT-IR spectra obtained upon NO admission at increasing pressure up to 2 mbar on Pd$_1$/SSZ-13 oxidized at 500 °C. The spectra are dominated by two bands at 1865 and 1806 cm^{-1} that increase in intensity upon increasing NO pressure. It is worth of note that, differently from CO, adsorbed NO is not able to separate the contributions related to Pd^{n+} ions in different coordination states (isolated ions and particles). For this reason the complex envelopes of bands present in the spectra of adsorbed CO do not have a correspondence in the spectral features obtained upon NO adsorption.

In any case, the observed bands at 1865 and 1806 cm^{-1} formed by NO adsorption are well documented in the literature although there is not a definitive consensus on their assignments. Some authors attributed the bands at 1865 and 1806 cm^{-1} as belonging to NO adsorbed in the form of nitrosyl species of Pd^{2+} and Pd$^+$, respectively [12,22]. However, recently Bell and co-workers [15], based on TPD and IR spectroscopy combined also with DFT calculations, indicated that the band at 1860 cm^{-1} has contributions from NO weakly adsorbed on Pd^{2+} and more strongly on Pd$^+$. This finding was consistent with DFT results of Mandal et al. [33], which revealed very similar frequencies for NO adsorbed on Pd^{2+} and Pd$^+$.
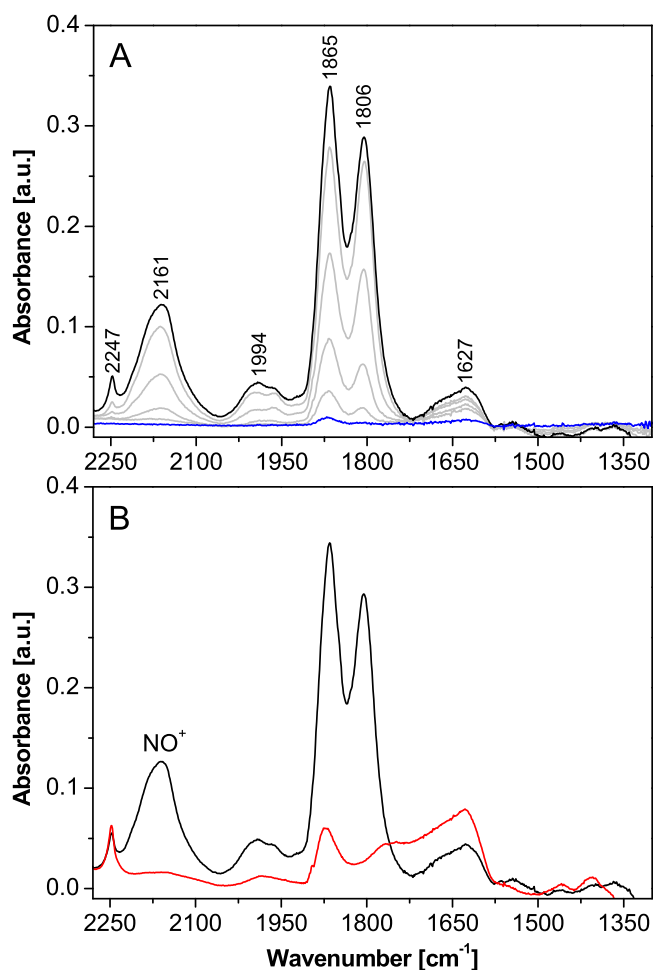
Fig. 6. - Panel A: FT-IR spectra of NO adsorbed at increasing pressure up to 2 mbar (from blue to black trace) and at r.t. on Pd$_1$/SSZ-13 pre-treated in O$_2$ at 500 °C. Panel B: comparison between the FT-IR spectra obtained after adsorption of 2 mbar of NO on Pd$_1$/SSZ-13 pre-treated in O$_2$ at 500 °C (black trace) and pre-treated in H$_2$ at 500 °C (red trace).

Along with nitrosyl bands, peaks at 2247, 2161, 1994 and 1627 cm^{-1} increase in intensity upon increasing NO coverage. The band at 2247 cm^{-1} and the envelope at about 1994 cm^{-1} are related to N$_2$O and N$_2$O$_3$, respectively, [48] present as impurities in the gas or formed as detailed below. On the other hands, the bands at 2162 and 1627 cm^{-1} are assigned to NO$^+$ and adsorbed molecular water, respectively. Hadjiivanov et al. proposed the formation of these species upon the reaction of NO with Brønsted acid sites of an H-ZSM-5 in the presence of oxygen [49] according to the following stoichiometry:

$$2\ NO + \tfrac{1}{2}\ O_2 + 2\ O_{lattice}–H^+ \rightarrow H_2O + 2\ O_{lattice}–NO^+ \quad (1)$$
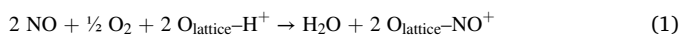
In our case oxygen is not present in the gas phase, and therefore it is reasonable to hypothesize the involvement of adsorbed oxygen species on the PdO$_x$ phase. Khivantsev et al. hypothesized that, without oxygen in the gas phase, nitrosonium ions are formed by Pd^{2+} reduction [12]. In Fig. 6 A bands related to Pd^{2+} and Pd$^+$ do not change their relative intensity during NO adsorption, but as previously discussed there might be an ambiguity in the exact assignments of these bands. Over Pd/FER, the same authors [16] suggested that PdO clusters can oxidize NO to NO$_2$, and that the formed NO$_2$ disproportionates to NO$^+$ and nitrates, whose presence is however not seen. Notably, the presence of adsorbed oxygen species on the pre-oxidized sample can also lead to the formation of NO$_2$ that, along with NO, can form the adduct N$_2$O$_3$ evidenced by the band at

1994 cm^{-1}, as reported above.

In Fig. 6 B the spectrum of NO adsorbed on the sample reduced at 500 °C (red trace) is compared with the spectrum obtained for the oxidized one (black trace). In the case of the reduced sample, no NO$^+$ formation is evidenced, highlighting that reaction (1) does not occur due to the lack of available oxygen species. Moreover, on the reduced sample, un-reduced Pd$^{2+/+}$ ions (band at 1865 cm^{-1}) are observed: in agreement with results obtained with CO adsorption on the reduced sample, this residual band is assigned to NO adsorbed on isolated Pd^{2+} ions stabilized by the zeolite framework. Nitrosyls of Pd^0 are not observed and the overall NO adsorption on the reduced sample is markedly lower than that observed for the oxidized one.

Accordingly, the overall results obtained by CO and NO adsorption at r.t. followed by FT-IR spectroscopy provide evidence in favor of the presence of Pd^{2+} and Pd$^+$ moieties (isolated or associated to PdO$_x$ particles) on oxidized sample. These species show noticeable stability (in dry conditions) to the reducing effect of CO.

3.2. Reactivity studies

3.2.1. NO$_x$ uptake at 150 °C

The NO$_x$ storage capacity of Pd$_1$/SSZ-13 has been evaluated in the temperature range 50–150 °C feeding NO in the presence of O$_2$, CO$_2$ and H$_2$O and the concentration profiles measured during the adsorption phase (phase 2) and the following TPD (phase 3) are shown in Fig. 7.

At 150 °C (Fig. 7 A), upon NO admission to the reactor (phase 2 in Fig. 7 A), the NO$_x$ (NO + NO$_2$) concentration increases rather slowly with time reaching the inlet concentration value after several minutes, thus indicating that NO$_x$ are adsorbed on the catalyst surface. NO$_x$ storage is accompanied by NO$_2$ evolution; the concentration of this species shows a peak and then decreases slowly to zero at the end of the storage, when the NO concentration approaches the inlet concentration value.

The overall amounts of NO$_x$ stored on the catalyst surface (estimated from the TPD curves) are shown in Fig. 8, splitted in the different temperature contributions that will be discussed later on. Fig. 8 also shows the calculated adsorbed NO$_x$/Pd molar ratios and the integral amounts of NO$_2$ evolved during the NO adsorption (phase 2) and during the subsequent TPD (phase 3).

At 150 °C temperature, 91.5 µmol/g$_{cat}$ of NO$_x$ are adsorbed on the catalyst, corresponding to a NO$_x$ / Pd molar ratio of 0.85. This indicates a very good adsorption efficiency, suggesting that Pd particles observed by TEM/HR-TEM measurements represent only a minor fraction of the Pd species present on the catalyst sample and/or participate to the NO$_x$ storage.

Complementary *operando* FT-IR experiments were also performed to analyze the nature and the evolution of the surface species originating during NO admission at 150 °C, and the results are shown in Fig. 9 A. Upon NO admission bands are formed at 1860 and 1808 cm^{-1}, which monotonically increase upon increasing the time on stream. These bands appears in the same positions of the bands obtained during the in-situ NO adsorption experiments previously reported (Fig. 6), and are hence attributed to Pd^{2+} and Pd$^+$ nitrosyls, respectively, although the contribution from Pd$^+$ sites for the IR feature at 1860 cm^{-1} cannot be ruled out. Notably, the position and the relative intensity of these bands are very similar to those observed in Fig. 6 A under dry conditions, although the *operando* runs have been carried out in the presence of water vapor and a partial hydration of the surface is apparent as pointed out by the small band at 1618 cm^{-1} related to the bending mode of adsorbed molecular water. This band is already present before feeding NO and is not significantly affected upon the NO storage. Of note, the spectra obtained under *operando* conditions show the absence of coordinated NO$^+$, characterized by the band near 2160 cm^{-1}, that on the other hand has been observed under dry conditions (see Fig. 6 A). This indicates that these species are displaced by water at the Brønsted acid sites [11].
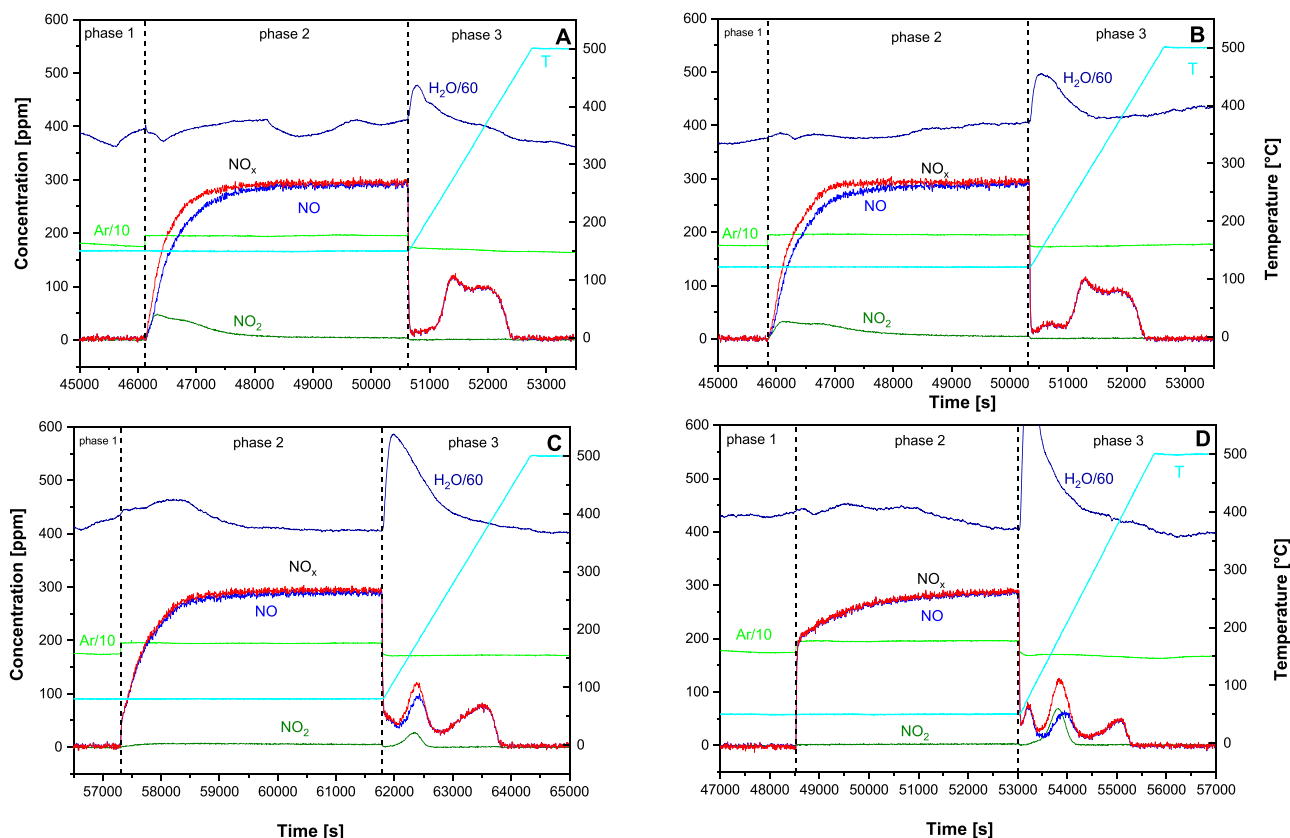
Fig. 7. - NO adsorption (phase 2) and subsequent TPD (phase 3) over Pd_1/SSZ-13 at different temperature: A) 150 °C, B) 120 °C, C) 80 °C, D 50 °C. Experimental conditions: storage phase (phase 2) NO (300 ppm) + O_2 (3%) + CO_2 (2%) + H_2O (2,5%) in He; TPD (phase 3) in O_2 (3%) + CO_2 (2%) + H_2O (2,5%) in He from 80 °C to 500 °C (10°/min).
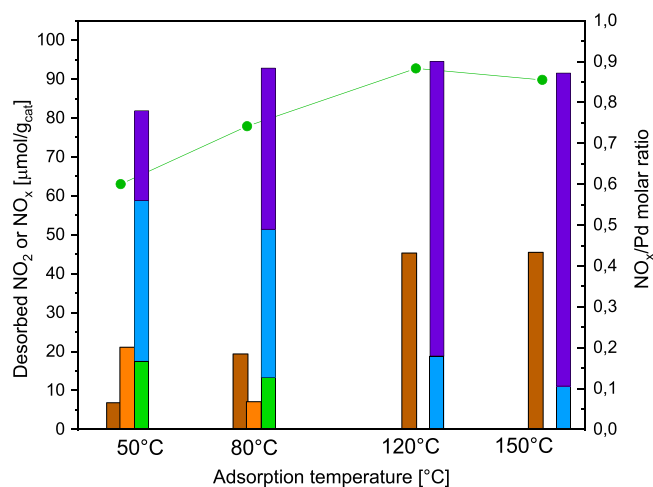

Fig. 8. - Amounts of NO_2 evolved during the adsorption phase (brown bar) and desorbed during the TPD phase (orange bar); amounts of NO_x desorbed during the TPD up to 120 °C (light green bar), from 120 °C to 240 °C (blue bar) and from 240 °C to 500 °C (violet bar); NO_x/Pd molar ratio (symbols) for different adsorption temperatures (amounts desorbed below 120°C neglected).

3.2.2. Mechanism of NO_x uptake

As previously observed, the NO_x storage is accompanied by a release of NO_2. This is in line with literature indications showing the generation of NO_2 during NO uptake [18,20,21,26,27,29,50,51]. In fact, it has been suggested that the NO uptake is not a simple adsorption process, but involves a two-step mechanism with an initial reduction of Pd^{2+} to Pd^+ by NO, followed by NO coordination onto Pd^+. Monomeric $[PdOH]^+$ are

envisaged as the storage sites (with Pd in the Pd^{2+} oxidation state, bonded to one Al and charge balanced by an OH group), and the evolution of NO_2 is associated to the reduction of Pd^{2+} to Pd^+ according to the stoichiometry of the following reaction (2) [18,20,21,26,27,29,50,51]:

$$2[PdOH]^+ + NO \rightarrow 2\,Pd^+ + NO_2 + H_2O \tag{2}$$

The reduced Pd^+ sites then coordinate NO forming Pd^+ nitrosyls, reaction (3):

$$2\,Pd^+ + 2\,NO \rightarrow 2\,Pd^+NO \tag{3}$$

The overall stoichiometry accounting for NO storage is hence provided by reaction (4):

$$2[PdOH]^+ + 3\,NO \rightarrow 2\,Pd^+NO + NO_2 + H_2O \tag{4}$$
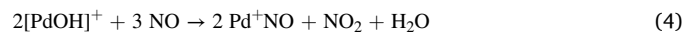
Zheng et al. [18] indicated that reaction (2) could be favored by water through solvation effects, which could enhance the mobility of $[PdOH]^+$ sites thus promoting reaction (2) (in fact two sites are needed to make NO oxidation feasible).

The same pathway, based on the reduction of Pd^{2+} to Pd^+ cations leading to the oxidation of NO to NO_2, was proposed to occur also over dimeric $[Pd\text{-}O\text{-}Pd]^{2+}$ sites, reaction (5) [18,30] or over dimeric $[PdOH]^+$ sites formed upon hydroxylation of monomeric $[PdOH]^+$ sites by water, reactions (6) and (7) [30,52]:

$$[Pd\text{-}O\text{-}Pd]^{2+} + NO \rightarrow 2\,Pd^+ + NO_2 \tag{5}$$

$$[Pd\text{-}O\text{-}Pd]^{2+} + H_2O \rightarrow [PdOH]^+\text{-}[PdOH]^+ \tag{6}$$

$$[PdOH]^+\text{-}[PdOH]^+ + NO \rightarrow 2\,Pd^+ + NO_2 + H_2O \tag{7}$$
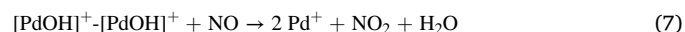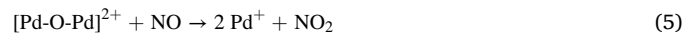
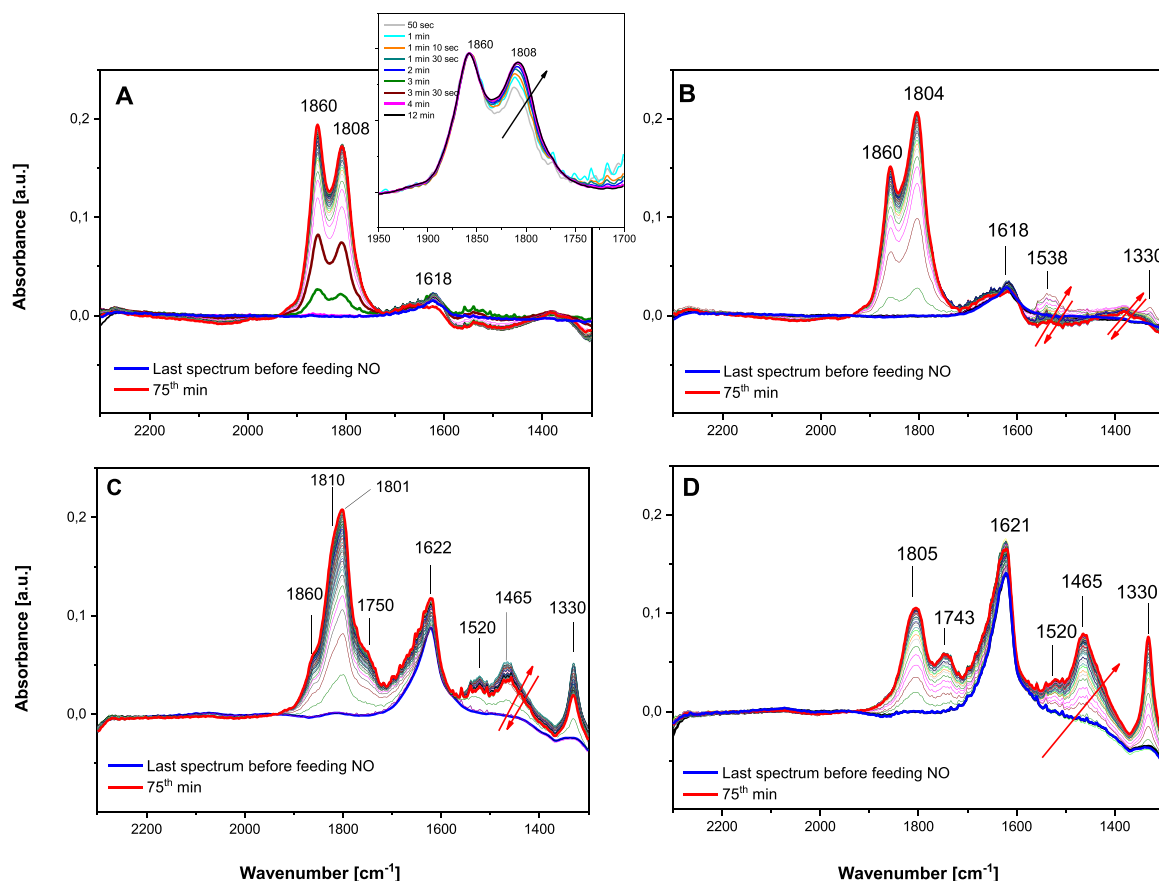In all cases, the NO uptake over Pd is described by a Pd^{2+} reduction

Fig. 9. - FT- IR spectra collected during the NO/O_2 adsorption at different temperature: A) 150 °C, B) 120 °C, C) 80 °C, D) 60 °C. Experimental conditions: storage phase NO (300 ppm) + O_2 (3%) + CO_2 (2%) + H_2O (1.5%) in He. Inset: spectra collected during the first 12 min of NO/O_2 exposure, normalized with the last spectrum collected after 75 min.

according to the overall reaction stoichiometry (4) and the storage process ends up with the formation of Pd^+ nitrosyls. Notably, reaction (4) implies the consumption of three molecules of NO with formation of two nitrosyl moieties and the release of one molecule of NO_2. The stoichiometry leads to a theoretical $NO_{2,evolved}/NO_{consumed}$ and $NO_{x,adsorbed}/NO_{consumed}$ ratios equal to 0.33 and 0.66, respectively. The actual values of these ratios have been estimated from the data of Fig. 7 and are shown as a function of time in Fig. 10 ($NO_{2,evolved}/NO_{consumed}$:
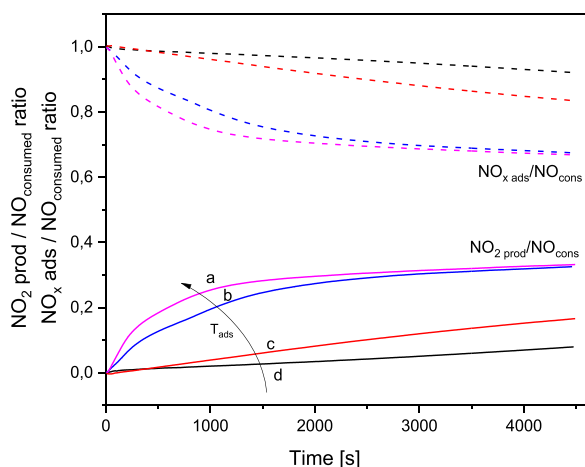

Fig. 10. - NO_2 produced in adsorption phase / NO consumed ratio (Solid lines); NO_x adsorbed / NO consumed ratio (Dash lines): 150 °C (a), 120 °C (b), 80 °C (c), 50 (d).

solid lines; $NO_{x,adsorbed}/NO_{consumed}$: dashed lines, respectively) at 150 °C (traces a) and at the other investigated temperatures. As apparent from Fig. 10, at 150 °C the $NO_{2,evolved}/NO_{consumed}$ and $NO_{x,adsorbed}/NO_{consumed}$ ratios expected form stoichiometry (4) are reached only at the end of the storage, and not during the initial part of the adsorption. In fact initially the $NO_{2,evolved}/NO_{consumed}$ ratio (trace a, solid line) is lower than the stoichiometric value of 0.33, while the $NO_{x,adsorbed}/NO_{consumed}$ ratio is higher than the stoichiometric one (0.66). In other words, during the initial part of the uptake, the amounts of evolved NO_2 are lower than those expected according to the stoichiometry of Eq. (4).

The observed deviations can be explained by assuming a fast initial NO uptake at the cationic Pd^{2+} sites (reaction (8)), before these sites are reduced, followed by the reduction of Pd^{2+} sites by stored NO with NO_2 release, reaction (9):

$$[PdOH]^+ + NO \rightarrow [PdOH]^+NO \tag{8}$$

$$[PdOH]^+NO + [PdOH]^+ \rightarrow 2\,Pd^+ + NO_2 + H_2O \tag{9}$$
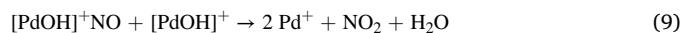
The process is then completed by the adsorption of NO on Pd^+ sites, previous reaction (3):

$$2\,Pd^+ + 2\,NO \rightarrow 2\,Pd^+NO \tag{3}$$

The sum of reactions (8)-(9) and (3) gives again the overall NO storage stoichiometry (4). The suggested pathway is in line with the results of FT-IR spectroscopy previously discussed (Fig. 9), showing the formation of Pd^{2+} nitrosyls upon NO admission. Alternatively, a slow NO_2 desorption process can also be invoked.

There are however other factors that may explain a departure from the overall stoichiometry of reaction (4). In fact, as pointed out by the

characterization study, Pd^+ sites are also initially present over the oxidized samples, along with Pd^{2+}. Pd^+ sites participate to the NO uptake according to the stoichiometry of reaction (3), with no evolution of NO_2, and this is expected to contribute to the observed deviations with respect to the overall stoichiometry of reaction (4). However, the observation that the stoichiometry of reaction (4) is respected at the end of the storage, indicates that the occurrence of reaction (3) cannot explain by itself the observed deviations.

In fact we have to recall that other sources of NO_2 can be present, and other factors may affect the Pd^{2+}/Pd^+ redox behaviour. As a matter of facts, it has been argued that NO_2 can be formed upon reaction of NO with oxidized Pd_xO_y species, reaction (10) [12,18]:

$$Pd_xO_y + NO \rightarrow Pd_xO_{y-1} + NO_2 \qquad (10)$$
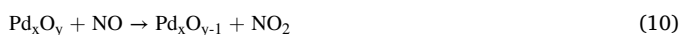
As a matter of facts, the reduction of PdO_2 to PdO accompanied by NO_2 formation was suggested by several studies [18,25,26,51]; the obtained PdO clusters/particles provide a possible pathway for NO_x storage resulting in the formation of PdO-NO species (reaction (11)) [18,20] and $PdNO_3$ species as well (reaction (12)) [25,26,51]:

$$PdO + NO \rightarrow PdO\text{-}NO \qquad (11)$$

$$PdO + 2NO + 3/2\ O_2 \rightarrow Pd(NO_3)_2 \qquad (12)$$

However, we note that formation of nitrates has not been observed at this temperature.

Summing up, it is apparent that different routes may be invoked to explain NO uptake and NO_2 release. The occurrence of these routes may provide a rationale for the observed deviations from the overall stoichiometry of reaction (4), at least during the initial part of the storage.

Notably, the stoichiometry of reaction (4) implies the massive Pd^{2+} to Pd^+ transformation occurring during the NO storage. We note that different literature studies assume the presence of only Pd^{2+} at the beginning of the NO uptake following an oxidative pretreatment [17,27, 29,34], and suggest that these Pd^{2+} species are eventually transformed into Pd^+ upon NO adsorption [27,29]. At variance, our characterization data suggest that Pd^+ species may be present even in the oxidized sample, along with Pd^{2+}. Besides, the complete reduction of Pd^{2+} by NO appears unlikely according to the results of the *operando* FT-IR measurements, and thanks to the presence of gas-phase oxygen during the experiments. To deepen this aspect, the spectra collected during the initial twelve minutes of the NO dose have been normalized with respect to the 1860 cm^{-1} band intensity, to analyse the changes in the relative intensities of the 1860 and 1808 cm^{-1} bands, associated to Pd^{2+} and Pd^+ nitrosyls, respectively. The results, shown in the inset of Fig. 9 A, point out that at the early stage of adsorption (i.e. during the first four minutes) the relative intensity of the 1808 cm^{-1} band related to Pd^+ nitrosyls increases with respect to the band at 1860 cm^{-1}, likely indicating the effective Pd^{2+} reduction to Pd^+. However, after 4 min the relative intensity of the Pd^{2+} and Pd^+ nitrosyl bands does not change anymore, suggesting the lack of a complete Pd^{2+} to Pd^+ interconversion. We note however that, if one assumes that Pd^+ nitrosyls contribute to the band at 1860 cm^{-1} as well, as suggested by Bell and co-workers [15, 28], the Pd^{2+} to Pd^+ transformation cannot be precisely monitored. Nevertheless, the spectra shown in the inset of Fig. 9 A can be hardly explained on the basis of a full interconversion of Pd^{2+} to Pd^+ sites that, therefore, seems unlikely under our experimental conditions. Besides, given that the NO adsorption is carried out in the presence of 3% O_2 v/v, the reoxidation of Pd^+ to Pd^{2+} is also possible. This has in fact shown by Bell and co-workers [28] who pointed out that the reoxidation of Pd^+ occurs even in the presence of trace amounts of O_2. Accordingly, this makes unlikely the extensive reduction of Pd^{2+} sites into Pd^+ during the NO storage in the presence of oxygen, as occurring under actual conditions.

3.2.3. Effect of temperature on NO_x uptake

The NO adsorption was carried also out at lower temperatures, i.e. 120 °C, 80 °C, and 50 °C. The corresponding gas phase and surface results are shown in Figs. 7B, 7 C and 7D and Figs. 9B, 9 C and 9D, respectively. When the NO adsorption is carried out at 120 °C and 80 °C (Figs. 7B and 7 C), the NO storage dynamics are very similar to the experiment performed at 150 °C, although lower amounts of NO_2 are released upon the NO adsorption at 80 °C (see also Fig. 8). At variance, at the lowest investigated temperature, i.e. 50 °C (Fig. 7D), the outlet NO concentration shows an initial step response followed by a slow increase to the inlet concentration value. The NO_x storage capacity is only slightly affected by temperature in the range 80–150 °C and is near 91–95 $\mu mol/g_{cat}$ (Fig. 8). Instead, lower amounts of NO_x were stored at 50 °C (i.e. near 82 $\mu mol/g_{cat}$).

The impact of temperature on the shape of the NO_2 evolution is significant. At 150 °C its concentration shows a maximum with time, as already discussed, but the curves become smoother with temperature and almost no NO_2 is detected at 50 °C. This could be explained with the kinetic dependence on temperature of the NO storage reaction, as also visible on the estimated $NO_{2,evolved}/NO_{consumed}$ and $NO_{x,adsorbed}/NO_{consumed}$ ratios (see Fig. 10) that in fact reach faster the asymptotic values upon increasing the temperature.

The results of the *operando* FT-IR experiments carried out at the same temperatures are displayed in Figs. 9B, 9 C and 9D (please note that the experiment in the *operando* cell at the lowest temperature has been carried out at 60 °C instead of 50 °C). At all the investigated temperatures a broad band at ca. 1620 cm^{-1} related to adsorbed water is present in the spectra, whose intensity increases on decreasing the temperature. This indicates that surface hydration increases at low temperatures, as expected.

At all the investigated temperatures IR features appear in the region 1900–1700 cm^{-1}, related to the formation of nitrosyl species; however, the IR features of such species changes with temperature, due to the different hydration degree. In particular, at the lowest investigated temperature (i.e. 60 °C, Fig. 9D) two bands are observed at 1805 and 1743 cm^{-1}, which are shifted to lower wavenumbers with respect of those observed at 150 °C. We can attribute the two IR features to $Pd^{2+}(NO)(H_2O)_x$ and $Pd^+(NO)(H_2O)_x$ complexes, respectively, in line with the increased surface hydration at 60 °C. In fact, according to the literature, the coordination of a water molecule to $Pd^{n+}NO$ complex is expected to decrease the NO stretching by ca. 50 cm^{-1} [50,53]. A similar red-shift for hydrated Pd^{2+} nitrosyls on Pd-zeolites has also been recently reported by other studies [11,33,54,55].

A more complex situation is apparent at intermediate temperatures. In fact, when the uptake is performed at 80 °C (Fig. 9 C) a main IR feature is visible centered at 1801 cm^{-1}, with three shoulders at 1860, 1810 and 1750 cm^{-1}. In line with the results obtained at 150 °C (see Fig. 9 A) the features at 1860 and 1810 cm^{-1} are assigned to nitrosyl species of Pd^{2+} and Pd^+. Instead, in accordance with the results obtained at 60 °C (see Fig. 9D) the features at 1801 and 1750 cm^{-1} are likely associated to nitrosyl species on hydrated Pd^{n+} cations. Accordingly, a variety of hydrated/anhydrous nitrosyls are present at such temperature. Finally, at 120 °C (Fig. 9B) bands develop again at 1860 cm^{-1} and 1804 cm^{-1}; however, their relative intensity is reversed if compared to the NO adsorption performed at 150 °C. This is likely ascribed to the higher hydration occurring at 120 °C than 150 °C.

Of note, upon decreasing the temperature, bands related to monodentate nitrates ($\nu_{asym}(NO_2)$ and $\nu_{sym}(NO_2)$ modes at 1465 cm^{-1} and 1330 cm^{-1}, respectively) and bidentate nitrates ($\nu(N=O)$ at 1520 cm^{-1}) develop. These bands are hardly visible at 150 °C. The position of these peaks is in agreement with those of Kunal et al. [54]. Nitrates formation increases upon decreasing the temperatures; at 60 °C (Fig. 9D) the bands of nitrates monotonically increase with time and at the end of the storage phase the intensity of the bands of the monodentate nitrates is comparable to those of nitrosyls. Instead, at 80 °C (Fig. 9 C) and 120 °C (Fig. 9B) the bands of nitrates initially increase and

then decrease with time, so that at 120 °C only nitrosyls are present on the catalyst surface at the end of the adsorption phase (phase 2). Formation of nitrates is instead negligible at 150 °C (Fig. 9 A).

These nitrate species are associated with the Pd phase, although it is not clear whether they involve the participation of isolated Pd^{n+} sites or PdO particles. These latter species have been suggested as possible sites for NO_x storage resulting in the formation of $Pd(NO_3)_2$ species, reaction (12) [20,21,25,26,51]:

$$PdO + 2NO + 3/2 \, O_2 \rightarrow Pd(NO_3)_2 \qquad (12)$$

The formation of nitrates may be also tentatively explained through the interaction of NO_2 that forms during the uptake and water, resulting in the formation of HNO_3 [56–58]:

$$3NO_2 + H_2O \rightarrow 2HNO_3 + NO \qquad (15)$$

The so-formed HNO_3 eventually leads to the formation of nitrates.

3.2.4. NO_x release

At the end of the adsorption phase, after the NO shutoff, the catalyst is heated (TPD) under He flowing in the presence of 2.5% H_2O and 3% O_2 (phase 3 in Fig. 7). In all cases the evolution of H_2O is observed during the initial part of the heating ramp; the intensity of the water peak increases upon decreasing the adsorption temperature, in line with the higher surface hydration at low temperatures (see above). Besides water, NO_x (NO and NO_2) are also seen to desorb from the surface with multiple NO_x desorption peaks.

When the adsorption has been carried out at high temperatures, i.e. 150 °C (Fig. 7 A) and 120 °C (Fig. 7B), only NO evolution is observed, taking place almost entirely at temperature above 200 °C showing a broad peak with two maxima near 280 °C and 370 °C.

Different NO_x desorption profiles are observed when the adsorption is performed at lower temperatures. After adsorption at 80 °C (Fig. 7 C) the NO_x desorption occurs with two main peaks, one centered at low temperature (i.e. 160 °C) and one at high temperature (i.e. 370 °C). The high temperature peak consists exclusively of NO, while minor amounts of NO_2 are observed in correspondence of the low temperature peak. Finally, when the adsorption is performed at the lowest investigated temperature, i.e. 50 °C (Fig. 7D), a low-temperature NO desorption peak centered at 80 °C is also observed, in addition to the high temperature peak. Most likely this low-T peak is due to the desorption of very weakly adsorbed (i.e. physisorbed) NO_x species.

The amounts of NO_x desorbed have been estimated considering that at temperature lower than 120 °C only physisorbed species desorb from the surface; then, two contributes have been distinguished, i.e. from 120 °C to 240 °C and above 240 °C; the results are shown in Fig. 8. It clearly appears that the lower the adsorption temperature, the lower the

thermal stability of the adsorbed NO_x species; in fact, the amounts of NO_x desorbed in the low temperature region (i.e. up to 240 °C) decreases upon increasing the adsorption temperature.

The presence of multiple NO_x desorption peaks points out to the existence of different NO_x surface species/different adsorption sites, having different thermal stability. To further address this point, FT-IR spectra were collected under *operando* conditions during the TPD runs as well, and results are displayed in Fig. 11. For the sake of clarity, the spectra are grouped in three temperature ranges, i.e. up to 230 °C, 230–350 °C, 350–500 °C.

In all cases upon the initial heating up to 230 °C, the band near 1620 cm^{-1}, assigned to adsorbed water, decreases and eventually disappears, indicating the dehydration of the surface. Concerning nitrosyls (in the region 1900–1700 cm^{-1}), the transformation of the hydrated $Pd^{n+}(NO)(H_2O)$ complexes into $Pd^{n+}(NO)$ nitrosyls is apparent: this transformation takes place only to a minor extent when the NO adsorption is performed at 150 °C (Fig. 11 A), in line to the very low surface hydration but is significant after adsorption at low temperatures. As a matter of fact, after adsorption at 80 °C (Fig. 11 C) and 60 °C (Fig. 11D), the band near 1750 cm^{-1} associated to $Pd^+(NO)(H_2O)$ complexes gradually decreases upon increasing the temperature up to 230 °C and eventually disappears. Similarly, also the band at ca. 1805 cm^{-1} partially associated to $Pd^{2+}(NO)(H_2O)$ complexes gradually decreases. In parallel the band at 1860 cm^{-1} related to $Pd^{2+}(NO)$, even if contribution of $Pd^+(NO)$ cannot be excluded, markedly increases with the increasing temperature. The conversion of hydrated nitrosyls into the corresponding anhydrous in the low temperature range of the TPD run (below 230 °C) is also confirmed by a well evident isosbestic point in the spectra.

Finally, nitrates (monodentate and bidentate) are also decomposed in the low temperature region. The bands of these species, observed in the region 1500–1300 cm^{-1}, are well evident in case of the adsorptions performed at 60 °C and 80 °C, rapidly decrease upon temperature increase and are almost completely removed below 200 °C. Decomposition of nitrates is accompanied by NO_2 release in the TPD profiles (Fig. 7).

At 230 °C, the features of the adsorbed NO_x species are similar for all NO adsorption temperatures, with nitrosyls present on the catalyst surface. Then, upon further increasing the temperature above 230 °C, in all cases the bands related to Pd^{n+} nitrosyls start to monotonically decrease and eventually disappear.

The surface concentration of nitrosyls and nitrates with temperature, obtained upon integration of the corresponding bands in the IR spectra of Fig. 11, is shown in Fig. 12. Nitrates (formed only upon NO adsorption at 60 and 80 °C) rapidly decrease and are almost complete removed at 200 °C. At variance, nitrosyls show a much higher stability. In
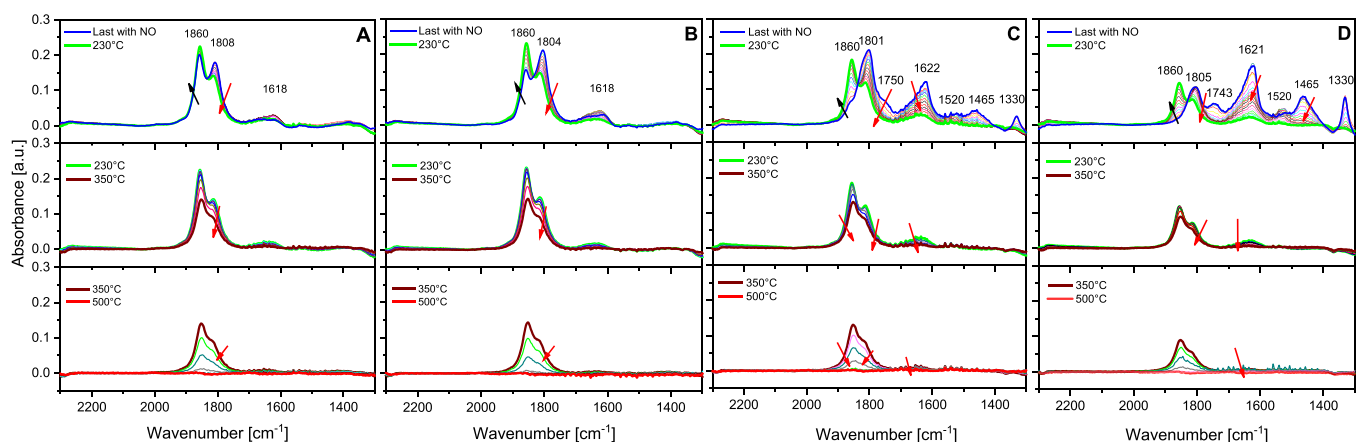

Fig. 11. - FT-IR spectra collected during the Temperature Programmed Desorption (TPD) after NO/O_2 adsorption at 150 °C (A), 120 °C (B), 80 °C (C), 60 °C (D). Experimental conditions: TPD in O_2 (3%) + CO_2 (2%) + H_2O (1.5%) in He from 80 °C to 500 °C (10°/min).
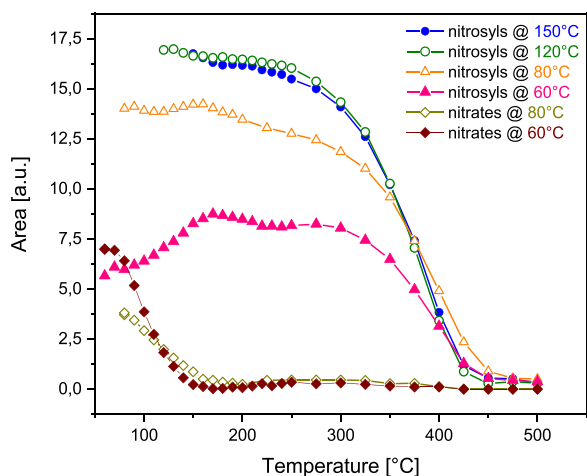
Fig. 12. - Trends of integrated area for (A) nitrosyls (1950–1710 cm^{-1}) and (B) nitrates (1570–1300 cm^{-1}) during TPD subsequent to NOx adsorption.

particular, the initial nitrosyls dehydration process and interconversion of hydrated into anhydrous nitrosyls does not lead to a significant decomposition of these species below 200 °C. Worth noticing that the nitrosyls surface concentration initially increases with temperature when adsorption is carried out at the lowest investigated temperature (60 °C), showing a maximum near 150 °C. This may be related to the decomposition of the surface nitrates to NO/NO$_2$ followed by NO re-adsorption on the Pd sites forming nitrosyls. Only upon further increases of the temperature above 200 °C, nitrosyls start to decrease and eventually disappear above 425 °C.

Accordingly, nitrates, whose formation is noticeable at low temperatures, are likely responsible for the low temperature NO$_x$ desorption, and are associated with the evolution of NO$_2$. On the other hand, the high temperature NO evolution in the TPD spectra corresponds to the decomposition of surface nitrosyls. Notably, two maxima near 280 °C and 370 °C are apparent in the high-temperature TPD peaks of Fig. 7 A and Fig. 7B. This calls for the presence of nitrosyls having different thermal stability. Based on DFT calculations, it has been suggested that Pd^{2+}-nitrosyls are less stable than Pd$^+$-nitrosyls [10,15,25,26,29], that can be hence responsible for the high temperature desorption feature. However, no clear evidences could be derived in this respect from the analysis of the FTIR spectra of Fig. 11 upon inspection of the relative intensities of the bands near 1860 cm^{-1} and 1805 cm^{-1} (associated to Pd^{2+} and Pd$^+$ nitrosyls, respectively) due to the suggested contribution of the Pd$^+$ nitrosyls to the 1860 cm^{-1} band [15] and to the oxidation phenomena likely occurring during the TPD run in the presence of oxygen.

3.2.5. Effect of the NO$_2$ presence

Since realistic engine exhausts do contain NO$_2$ in addition to NO, the effect of the presence of NO$_2$ on the NO$_x$ storage has been investigated. Accordingly, experiments have been performed adding NO$_2$ (50 ppm or 100 ppm) to NO/O$_2$ mixture while the total NO$_x$ concentration has been maintained equal to 300 ppm. Experiments have been performed at 80 °C, and results are shown in Fig. 13 (gas phase) and 14 (surface phase). In Fig. 13 A the data obtained in the absence of NO$_2$ and already presented in Fig. 7 C have also been shown for comparison purposes.

Fig. 13B shows the results obtained with a NO$_2$ / NO molar ratio equal to 0.2. Upon NO$_x$ admission, both the NO and NO$_2$ concentrations increase slowly reaching the inlet value at the end of the storage phase. Then, after the NO$_x$ shutoff and upon heating the sample (phase 3), the desorption of NO$_x$ is observed, due to the decomposition of the stored species. Two desorption peaks are observed, i.e. at low temperature centered at 170 °C where NO$_x$ desorb mainly in the form of NO$_2$, and a second broad peak at higher temperature with maximum centered near
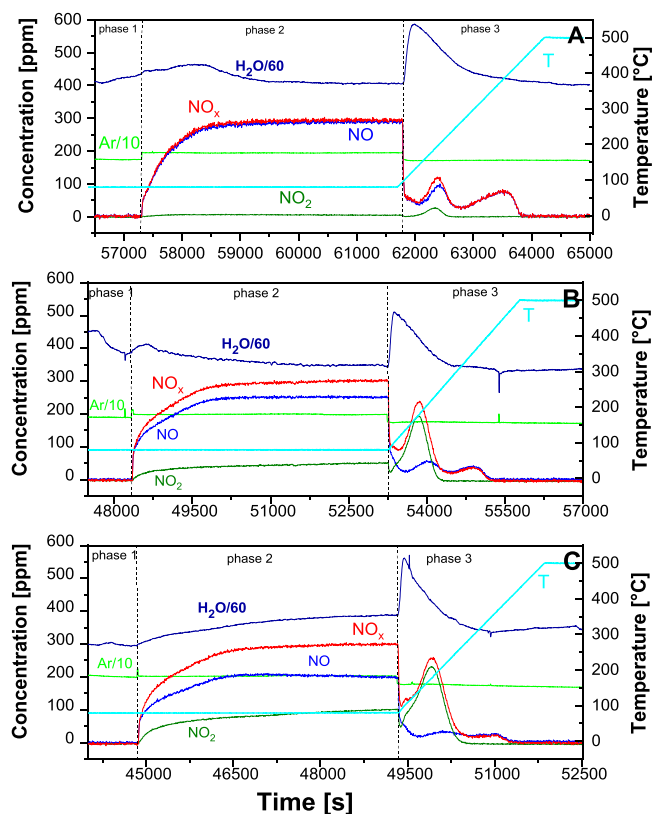

Fig. 13. - NO/NO$_2$/O$_2$ adsorption (phase 2) and subsequent TPD (phase 3) at 80 °C over Pd$_1$/SSZ-13. A) NO$_2$ / NO ratio = 0; B) NO$_2$ / NO ratio = 0.2; C) NO$_2$ / NO ratio = 0.5. Experimental conditions: storage phase NO (300, 250 or 200 ppm) + NO$_2$ (0, 50 ppm or 100 ppm) + O$_2$ (3%) + CO$_2$ (2%) + H$_2$O (2.5%) in He. TPD in O$_2$ (3%) + CO$_2$ (2%) + H$_2$O (2.5%) in He from 80 °C to 500 °C (10°/min).

370 °C and formed exclusively by NO. The total amount of desorbed NO$_x$ was estimated and increased by ca.15% if compared with the experiment performed in the absence of NO$_2$.

Inspection of Fig. 13 shows that the presence of NO$_2$ has a pronounced impact on both the amounts of stored NO$_x$ and on the stability of the adsorbed species. The amounts of adsorbed NO$_x$ increases upon increasing the NO$_2$ concentration in the feed (from 93 μmol/g$_{cat}$ in the absence of NO$_2$ up to 113 μmol/g$_{cat}$ with NO$_2$/NO molar ratio equal to 0.5), and the thermal stability of the adsorbed species decreases. In fact, the high temperature desorption peak progressively decreases in intensity while the low temperature peak, corresponding to the evolution mainly of NO$_2$, increases with temperature.

The presence of NO$_2$ impacts the nature of the adsorbed surface species with respect to the pure NO feed, as revealed by *operando* FT-IR analysis whose results are displayed in Fig. 14. In particular, the spectra obtained with a NO$_2$/NO molar ratio equal to 0.2 are shown in Fig. 14 A, where the spectrum recorded in the absence of NO$_2$ at the end of the storage is also reported as dotted line for comparison purposes (the whole series of spectra is shown in Fig. 9 C). In the presence of NO$_2$, the bands of Pd nitrosyls (in the region 1900–1800 cm^{-1}) are still observed but with lower intensities with respect to that obtained in the presence of only NO/O$_2$ (see dotted line reported in Fig. 14 A). Moreover, in this case, the bands of nitrosyls initially increase and then decrease, so that their presence is almost negligible at the end of the storage. At variance with the NO$_2$-free experiment, the significant formation of bands in the region 1500–1300 cm^{-1} is observed, corresponding to surface nitrates. In particular, the bands at 1460 cm^{-1} and 1330 cm^{-1} are related to monodentate nitrates while the band at 1520 cm^{-1} is assigned to bidentate nitrates. Besides co-adsorption of NO/NO$_2$ leads also to the
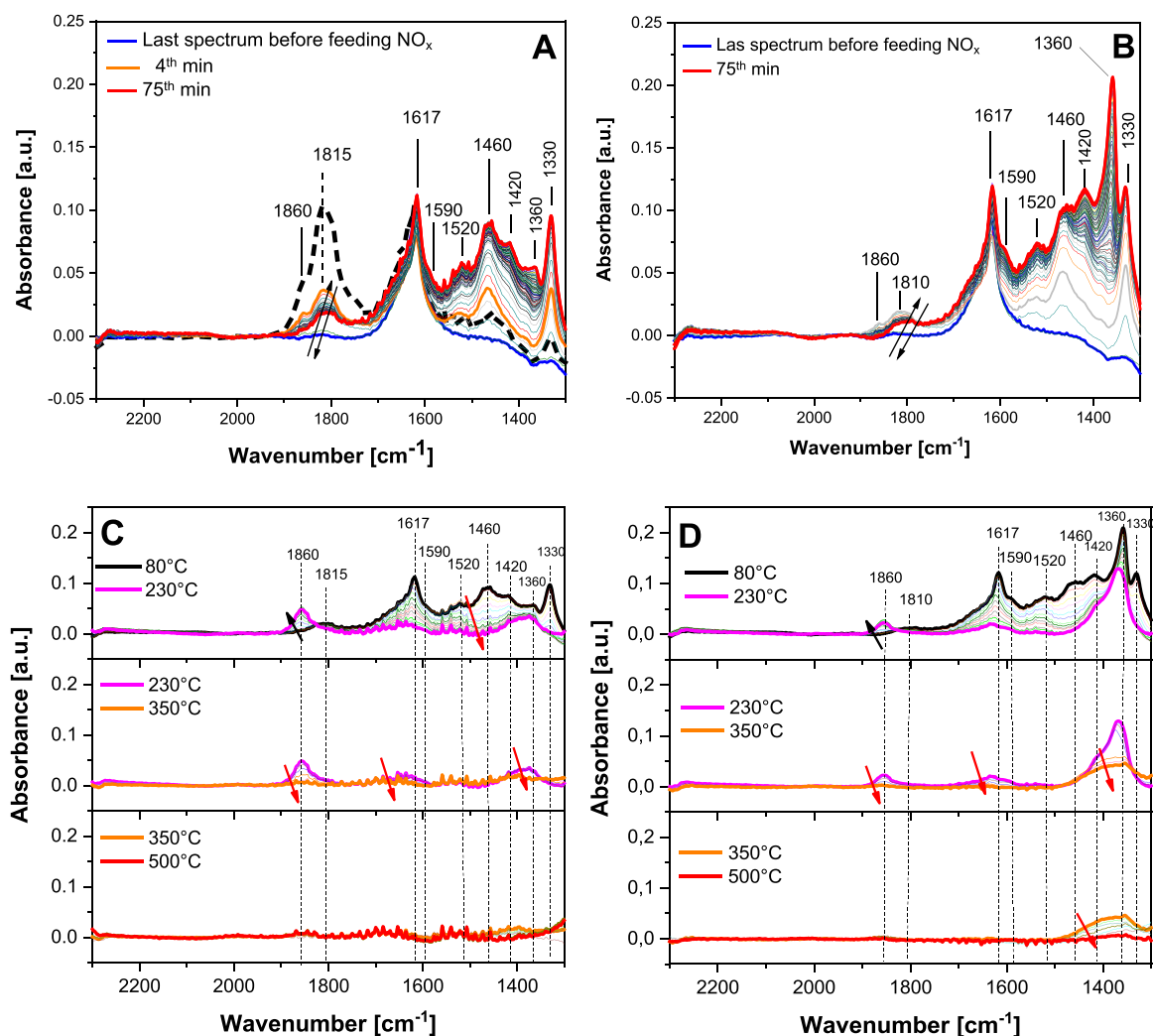
Fig. 14. - FT-IR spectra collected during the $NO/NO_2/O_2$ adsorption at 80 °C (A) NO_2 / NO ratio = 0.2; B) NO_2 / NO ratio = 0.5) and subsequent TPD (C and D, respectively). Experimental conditions: storage phase NO (250 or 200 ppm) + NO_2 (50 ppm or 100 ppm) + O_2 (3%) + CO_2 (2%) + H_2O (1.5%) in He. TPD in O_2 (3%) + CO_2 (2%) + H_2O (1.5%) in He from 80 °C to 500 °C (10°/min). Dotted spectrum reported in Fig. 14 A refers to NO/O_2 adsorption at 80 °C (i.e. without NO_2).

appearance of new bands at 1420 and 1360 cm^{-1} that will be discussed in the following. Finally, the band at 1617 cm^{-1} is due to the bending mode of adsorbed molecular water. In this case, however, the presence of a shoulder at 1590 cm^{-1} related to bidentate nitrates is also apparent, which have not been observed in the presence of only NO.

When the NO_2/NO molar ratio is increased up to 0.5 (Fig. 14B), the spectra closely resemble that already described for the experiment with a lower NO_2/NO molar ratio. However, upon increasing the NO_2 concentration an increase in the bands at 1420 and 1360 cm^{-1} is observed, at the expenses of nitrosyls whose formation is very small. A comparison of Fig. 14 A with Fig. 14B points out that the bands at 1420 and 1360 cm^{-1} do not correlate, being their intensity ratio very different in the two cases. In particular, the band at 1360 cm^{-1} is very intense in Fig. 14B and is very near to that of nitrate ion in salts ($\nu_{asym.}(NO_3)$ mode at 1380–1370 cm^{-1}), i.e. bulk nitrates [48]. For this reason, it is tentatively assign to subsurface ("bulk") nitrates formed on the PdO_x particles present on the external surfaces of the zeolite. This assignment is coherent with the thermal stability of this species observed during TPD reported in the following. On the other hand, the band at 1420 cm^{-1} is assigned to the $\nu_{asym.}(NO_2)$ mode of nitro compounds [48], such as Pd^{n+}-NO_2, with the corresponding $\nu_{sym.}(NO_2)$ mode that falls in the same region of the $\nu_{asym.}(NO_3)$ mode of "bulk" nitrates.

FT-IR spectra collected during the TPD run after NO_x adsorption with NO_2/NO molar ratio of 0,2 and 0,5 are shown in Fig. 14 C and Fig. 14D,

respectively. In both cases, the spectra recorded during the initial heating of the catalysts (i.e. up to 230 °C), show the growth of the band at 1860 cm^{-1}, related to the Pd^{2+}(NO) nitrosyls, along with surface dehydration, pointed out by the decrease of the band at ca. 1620 cm^{-1}, assigned to adsorbed water. The increase of the band at 1860 cm^{-1} related to the Pd^{2+}(NO) nitrosyls can be partially ascribed to the dehydration of $Pd^{n+}(NO)(H_2O)$ complexes (small band at 1815 cm^{-1}), but also to NO readsorption formed upon nitrate decomposition at low temperatures. In fact, the bands of monodentate nitrates at 1465 cm^{-1} and 1330 cm^{-1} and of bidentate nitrates at 1520 cm^{-1} rapidly decrease upon heating and they are almost completely removed below 230 °C. Decomposition of nitrates leads to NO and NO_2 evolution at low temperature seen in the gas phase (Fig. 13), possibly leading to the formation of nitrosyls.

At variance, the bands at 1360 and 1420 cm^{-1}, associated to subsurface nitrates and nitro compounds, respectively, remains almost unchanged up to 230 °C. The high thermal stability of subsurface nitrates is expected. As for the nitro compounds (band at 1420 cm^{-1}), the high thermal stability could be related to the formation inside the zeolite channels on Pd^{n+} isolated ions.

Upon further increasing the temperature above 230 °C the bands related to Pd^{n+} nitrosyls start to monotonically decrease and then disappear at ca. 300 °C. Also the bands at 1420 and 1360 cm^{-1} start to decrease and eventually disappears at ca. 350 °C and 450 °C (Fig. 14 C

and Fig. 14D, respectively). This leads to the high-T evolution of NO seen in the TPD profiles of Figs. 13B and 13 C.

Hence the data clearly indicates that the presence of NO_2 in the feed stream inhibits the formation of nitrosyls leading to the formation of poorly stable surface nitrates, of subsurface nitrates and of nitro-compounds as well. The surface nitrates decompose at low temperature (below 250 °C) leading to NO_2 (and NO) evolution, and also to the formation of small amounts of nitrosyls. These latter decompose at higher temperatures, along with subsurface nitrates and nitro-compounds, leading to NO evolution in the gas phase.

4. Conclusions

This study has addressed the pathways involved in the NO_x adsorption on Pd_1/SSZ-13, particularly focusing on the nature, stability and reactivity of the adsorbed NO_x species. For this purpose, a Pd_1/SSZ-13 catalyst has been synthesised and characterized, and the adsorption/ decomposition of NO/NO_2 mixtures has been analysed under relevant conditions, i.e. in the presence of water and CO_2.

As shown by in-situ CO/NO adsorptions followed by FT-IR spectroscopy, the synthesized oxidized catalyst shows the presence of isolated Pd^+ and Pd^{2+} species, formed by ion exchange with the Brønsted acid sites of the zeolite, and PdO_x particles on the external surface of the zeolite. Based on the relative intensities of the Pd FTIR bands, Pd^{2+} isolated ions are the most abundant species on the freshly calcined sample.

Upon contact with NO under actual conditions, formation of nitrosyls on both Pd^+ and Pd^{2+} sites is observed, along with minor amounts of nitrates at low temperatures (i.e., at 50 and 80 °C). Nitrosyl formation does not occur through a simple NO adsorption reaction but a concomitant NO_2 evolution is observed. In particular, the overall amounts of NO_x stored (in the form of nitrosyls) and of NO_2 evolved obey the stoichiometry of the following reaction suggested in the literature:

$$2[PdOH]^+ + 3\,NO \rightarrow 2\,Pd^+NO + NO_2 + H_2O \qquad (4)$$
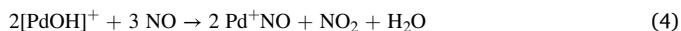
which implies the reduction of Pd^{2+} to Pd^+ by NO. Notably, the stoichiometry of reaction (4) is not accounted during the whole storage, since initially the amounts of NO_x stored overcome the amounts of NO_2 formed according to reaction (4) (and are lower near the end of the storage). This may suggest a fast NO uptake and/or a lower NO_2 release. Besides, no direct evidence could be obtained for the suggested massive reduction of Pd^{2+} to Pd^+, possibly due to the overlapping of the IR bands of Pd^{2+} and Pd^+, although it is also likely that the presence of oxygen reoxidizes Pd^+ to Pd^{2+}.

The same pathway is operating at all investigated temperatures, in the range 50–150 °C; however, at the lowest investigated temperatures the formation nitrates on Pd sites is also observed. The overall amounts of adsorbed NO_x does not change significantly with temperature; however, at low temperatures the fraction of nitrates increases at the expenses of nitrosyls.

The adsorbed NO_x species decompose upon heating, with evolution of NO and NO_2. Notably, the higher the adsorption temperature, the higher the fraction of evolved NO_x at high temperatures. This has been attributed to the formation of nitrates at low temperatures, that decompose at low temperature with evolution of NO and NO_2. At variance, the nitrosyls exhibit higher thermal stability. The interconversion of hydrated nitrosyl into anhydrous nitrosyls is observed at low temperatures upon heating, without a significant decomposition to NO; in fact the anhydrous nitrosyls decompose at high temperatures, in the range 200–400 °C with evolution of NO only.

The effect of the presence of NO_2 in the feed stream has also been addressed. It has been found that the formation of nitrosyls is inhibited in the presence of NO_2 in the feed, while the formation of poorly stable surface nitrates, of subsurface ("bulk") nitrates and of nitro-compounds

as well is observed. Hence the presence of NO_2 significantly affects the nature and stability of the adsorbed species. In fact, the surface nitrates decompose at low temperature (below 250 °C) leading to NO_2 (and NO) evolution, along with the formation of small amounts of nitrosyls. These latter decompose at higher temperatures, along with subsurface nitrates and nitro-compounds leading to NO evolution.

CRediT authorship contribution statement

R. Matarrese: Investigation, Writing – original, Conceptualization. **L. Castoldi:** Investigation, Writing – review & editing, Methodology. **S. Morandi:** Investigation, Writing – original, Conceptualization. **P. Ticali:** Investigation, Methodology. **M. C. Valsania:** Investigation, Formal analysis. **L. Lietti:** Supervision, Funding acquisition, Writing – review & editing.

Declaration of Competing Interest

The authors declare that they have no known competing financial interests or personal relationships that could have appeared to influence the work reported in this paper.

Data availability

Data will be made available on request.

References

[1] W.S. Epling, L.E. Campbell, A. Yezerets, N.W. Currier, J.E. Parks, Catal. Rev. 46 (2004) 163–245.
[2] A.M. Bale, F. Gao, I. Lezcano-Gonzalez, C.H.F. Peden, J. Szanyi, Chem. Soc. Rev. 44 (2015) 7371–7405.
[3] J.R. Gonzalez-Velasco, R. Lopez-Fonseca, B. Pereda-Ayo, N.S.R. Technology, in: L. Lietti, L. Castoldi (Eds.), NOx Trap Catalysts and Technologies: Fundamentals and Industrial Applications, Chapter 2, Royal Society of Chemistry, London, 2018, pp. 36–66.
[4] C.K. Lambert, React Chem, Eng 4 (2019) 969–974.
[5] A. Joshi, S.A.E. Technical, Paper 2021 (2021) 01–0575.
[6] H.Y. Chen, S. Mulla, E. Weigert, K. Camm, T. Ballinger, J. Cox, P. Blakeman, SAE Int. J. Fuels Lubr. 6 (2013) 372–381.
[7] J.R. Theis, C.K. Lambert, Catal. Today 258 (2015) 367–377.
[8] J. Lee, J.R. Theis, E.A. Kyriakidou, Appl. Catal. B Environ. 243 (2019) 397–414.
[9] Y. Gu, W.S. Epling, Appl. Catal. A Gen. 570 (2019) 1–14.
[10] H. Zhao, A.J. Hill, L. Ma, A. Bhat, G. Jing, J.W. Schwank, Catal. Sci. Technol. 11 (2021) 5986–6000.
[11] H.Y. Chen, J.E. Collier, D. Liu, L. Mantarosie, D. Duran-Martin, V. Novak, R. R. Rajaram, D. Thompsett, Catal. Lett. 146 (2016) 1706–1711.
[12] K. Khivantsev, F. Gao, L. Kovarik, Y. Wang, J. Szanyi, J. Phys. Chem. C. 122 (2018) 10820–10827.
[13] J. Lee, Y. Ryou, S. Hwang, Y. Kim, S.J. Cho, H. Lee, C.H. Kim, D.H. Kim, Catal. Sci. Technol. 9 (2019) 163–173.
[14] S. Yasumura, T. Ueda, H. Ide, K. Otsubo, C. Liu, N. Tsunoji, T. Toyao, Z. Maeno, K. Shimizu, Phys. Chem. Chem. Phys. 23 (2021) 22273–22282.
[15] P. Kim, J. Van der Mynsbrugge, H. Aljama, T.M. Lardinois, R. Gounder, M. Head-Gordon, A.T. Bell, Appl. Catal. B Environ. 304 (2022), 120992.
[16] I. Song, K. Khivantsev, Y. Wu, M. Bowden, Y. Wang, J. Szanyi, Appl. Catal. B Environ. 318 (2022), 121810.
[17] K. Khivantsev, X. Wei, L. Kovarik, N.R. Jaegers, E.D. Walter, R. Tran, Y. Wang, J. Szanyi, Angew. Chem. Int. Ed. 61 (2022), e202107554.
[18] Y. Zheng, L. Kovarik, M.H. Engelhard, Y. Wang, Y. Wang, F. Gao, J. Szanyi, J. Phys. Chem. C. 121 (2017) 15793–15803.
[19] J. Lee, Y.S. Ryou, S.J. Cho, Hg Lee, C. H. Kim., D. H. Kim., Appl. Catal. B Environ. 226 (2018) 71–82.
[20] A. Wang, K. Lindgren, M. Di, D. Bernin, P.A. Carlsson, Ma. Thuvander, L. Olsson, Appl. Catal. B Environ. 278 (2020), 119315.
[21] D. Yao, R. Feizie Ilmasani, J.C. Wurzenberger, T. Glatz, J. Han, A. Wang, D. Creaser, L. Olsson, Chem. Eng. J. 428 (2022), 132459.
[22] K. Khivantsev, N.R. Jaegers, L. Kovarik, J.C. Hanson, F. Tao, Y. Tang, X. Zhang, I. Z. Koleva, H.A. Aleksandrov, G.N. Vayssilov, Y. Wang, F. Gao, J. Szanyi, Angew. Chem. Int. Ed. 57 (2018) 16672–16677.
[23] Y. Ryou, J. Lee, S.J. Cho, H. Lee, C.H. Kim, D.H. Kim, Appl. Catal. B Environ. 212 (2017) 140–149.
[24] Y. Ryu, J. Lee, Y. Kim, S. Hwanga, H. Lee, C.H. Kim, D.H. Kim, Appl catal, A Gen. 569 (2019) 28–34.
[25] M. Ambast, K. Karinshak, B.M.M. Rahman, L.C. Grabow, M.P. Harold, Appl. Catal. B Environ. 269 (2020), 118802.
[26] A. Gupta, S.B. Kang, M.P. Harold, Catal. Today 360 (2021) 411–425.

[27] M. Ambast, A. Gupta, B.M.M. Rahman, L.C. Grabow, M.P. Harold, Appl. Catal. B Environ. 286 (2021), 119871.

[28] P. Kim, J. Van der Mynsbrugge, M. Head-Gordon, A.T. Bell, J. Phys. Chem. C. This: J. Phys. Chem. C. 126 (2022) 18744–18753.

[29] R. Villamaina, U. Iacobone, I. Nova, E. Tronconi, M.P. Ruggeri, L. Mantarosie, J. Collier, D. Thompsett, Appl. Catal. B Environ. 284 (2021), 119724.

[30] M. Kaushik, G. Shrivastav, T.S. Khan, M.A. Haider, D. Bhatia, Langmuir 37 (2021) 13799–13809.

[31] K. Chakarova, E. Ivanova, K. Hadjiivanov, D. Klissurski, H. Knözinger, Phys. Chem. Chem. Phys. 6 (2004) 3702–3709.

[32] I. Song, K. Khivantsev, Y. Wang, J. Szanyi, J. Phys. Chem. C. 126 (2022) 1439–1449.

[33] K. Mandal, Y. Gu, K.S. Westendorff, S. Li, J.A. Pihl, L.C. Grabow, W.S. Epling, C. Paolucci, ACS Catal. 10 (2020) 12801–12818.

[34] K. Khivantsev, N.R. Jaegers, I.Z. Koleva, H.A. Aleksandrov, L. Kovarik, M. Engelhard, F. Gao, Y. Wang, G.N. Vayssilov, J. Szanyi, J. Phys. Chem. C. 124 (2020) 309–321.

[35] L. Castoldi, R. Matarrese, S. Morandi, P. Ticali, L. Lietti, Catal. Today 360 (2021) 317–325.

[36] R.B. Pace, T.M. Lardinois, Y. Ji, R. Gounder, O. Heintz, M. Crocker, A.C.S. Omega 6 (2021) 29471–29482.

[37] J. Van der Mynsbrugge, M. Head-Gordon, A. Bell, J. Mater. Chem. A 9 (2021) 2161–2174.

[38] A. Porta, T. Pellegrinelli, L. Castoldi, R. Matarrese, S. Morandi, S. Dzwigaj, L. Lietti, Top. Catal. 61 (2018) 2021–2034.

[39] Collection of Simulated XRD Powder Patterns for Zeolites, Editors M.M.J. Treacy and J.B. Higgins, Fourth Revised Edition ELSEVIER, 2001.

[40] A.W. Aylor, L.J. Lobree, J.A. Reimer, A.T. Bell, J. Catal. 172 (1997) 453–462.

[41] K.I. Hadjiivanov, G.N. Vayssilov, Adv. Catal. 47 (2002) 307–511.

[42] B. Onida, F. Geobaldo, F. Testa, F. Crea, E. Garrone, Micro Mesopor. Mat. 30 (1999) 119–127.

[43] E. Groppo, S. Bertarione, F. Rotunno, G. Agostini, D. Scarano, R. Pellegrini, G. Leofanti, A. Zecchina, C. Lamberti, J. Phys. Chem. C. 111 (2007) 7021–7028.

[44] A. Bensalem, J.C. Muller, D. Tessier, F. Bozon-Verduraz, J. Chem. Soc. Faraday Trans. 92 (1996) 3233–3237.

[45] P. Ruzzi, Appl Catal, A Gen. 635 (2022), 118568.

[46] A. Zecchina, L. Marchese, S. Bordiga, C. Pazè, E. Gianotti, J. Phys. Chem. B 101 (1997) 10128–10135.

[47] I. Lezcano-Gonzales, U. Deka, B. Arstad, A. Van Yperen-De Deyna, K. Hemelsoet, M. Waroquier, V. Van Speybroeck, B.M. Weckhuysen, A.M. Beale, Phys. Chem. Chem. Phys. 16 (2014) 1639–1650.

[48] K.I. Hadjivanov, Catal. Rev. 42 (2000) 71–144.

[49] K.I. Hadjivanov, J. Saussey, J.L. Freysz, J.C. Lavalley, Catal. Lett. 52 (1998) 103–108.

[50] C. Descorme, P. Gelin, M. Primet, C. Lecuyer, Catal. Lett. 41 (1996) 133–138.

[51] S.A. Malamis, M.P. Harold, Catal. Today 360 (2021) 388–400.

[52] D. Mei, F. Gao, J. Szanyi, Y. Wang, Appl Catal, A Gen. 569 (2019) 181–189.

[53] L.J. Lobree, A.W. Aylor, J.A. Reimer, A.T. Bell, J. Catal 181 (1999) 189–204.

[54] P. Kunal, T.J. Toops, M.K. Kidder, M.J. Lance, Appl. Catal. B Environ. 299 (2021), 120591.

[55] Y. Gu, S. Sinha Majumdar, J. A. Pihl, W. S. Epling, Appl. Catal. B Environ. 298 (2021), 120561.

[56] J. Szanyi, J.H. Kwak, C.H.F. Peden, J. Phys. Chem. B 108 (2004) 3746–3753.

[57] R. Brosius, D. Habermacher, J.A. Martens, L. Vradman, M. Herskowitz, L. Capek, Z. Sobalik, J. Dedecek, B. Wichterlova, V. Tokarova, O. Gonsiorova, Top. Catal. 30 (2004) 333–339.

[58] M. Colombo, I. Nova, E. Tronconi, Appl. Catal. B Environ. 111–112 (2012) 433–444.